4648

Final Report • February 1995

InTlSb AS A LONG-WAVE INFRARED (LWIR) MATERIAL: DEFECTS AND TRANSPORT PROPERTIES

S. Krishnamurthy, Senior Research Physicist
M. van Schilfgaarde, Senior Research Physicist
M.A. Berding, Senior Research Physicist
A. Sher, Associate Director
Physical Electronics Laboratory

SRI Project 4648

Prepared for:

Scientific Officer
George Wright
Office of Naval Research
800 North Quincy Street
Arlington, VA 22217-5000

Attn: GW, Code: 1114SS

Contract N00014-93-C-0091

4648

Final Report • February 1995

InTlSb AS A LONG-WAVE INFRARED (LWIR) MATERIAL: DEFECTS AND TRANSPORT PROPERTIES

S. Krishnamurthy, Senior Research Physicist
M. van Schilfgaarde, Senior Research Physicist
M.A. Berding, Senior Research Physicist
A. Sher, Associate Director
Physical Electronics Laboratory

SRI Project 4648

Prepared for:

Scientific Officer
George Wright
Office of Naval Research
800 North Quincy Street
Arlington, VA 22217-5000

Attn: GW, Code: 1114SS

Contract N00014-93-C-0091

Approved:

Eric Pearson, Director
Physical Electronics Laboratory

Donald L. Nielson, Vice President
Computing and Engineering Sciences Division

SRI International 333 Ravenswood Avenue • Menlo Park, CA 94025-3493 • (415) 326-6200 • FAX: (415) 326-5512 • Telex: 334486

REPORT DOCUMENTATION PAGE

Form Approved
OMB No. 0704-0188

1. AGENCY USE ONLY (Leave Blank)	2. REPORT DATE	3. REPORT TYPE AND DATES COVERED
	February 1995	Final Report, 19 April 1993–14 January 1995

4. TITLE AND SUBTITLE

InTlSb as a Long-Wave Infrared (LWIR) Material: Defects and Transport Properties

5. FUNDING NUMBERS

6. AUTHORS

S. Krishnamurthy, M. van Schilfgaarde, M.A. Berding, and A. Sher

7. PERFORMING ORGANIZATION NAME(S) AND ADDRESS(ES)

SRI International
333 Ravenswood Avenue
Menlo Park, CA 94025-3493

8. PERFORMING ORGANIZATION REPORT NUMBER

4648

9. SPONSORING/MONITORING AGENCY NAME(S) AND ADDRESS(ES

Office of Naval Research
800 North Quincy Street
Arlington, VA 22217-5000

10. SPONSORING/MONITORING AGENCY REPORT NUMBER

11. SUPPLEMENTARY NOTES

12a. DISTRIBUTION/AVAILABILITY STATEMENT

Approved for public release; distribution unlimited

12b. DISTRIBUTION CODE

13. ABSTRACT *(Maximum 200 words)*

We have evaluated three III-V semiconductor alloys—$In_{1-x}Tl_xP$ (ITP), $In_{1-x}Tl_xAs$ (ITA), and $In_{1-x}Tl_xSb$ (ITS)—as possible candidates for future long-wave infrared (LWIR) detector materials. The cohesive energies, elastic constants, band structures, electron mobilities, and phase diagrams are calculated and are compared to those of $Hg_{1-x}Cd_xTe$ (MCT) alloys. All three of these III-V alloys have their band gap change from negative to positive values as the alloy composition x decreases from 1 to 0. The x values for the 0.1-eV gap are estimated to be 0.67, 0.15, and 0.08, respectively, for ITP, ITA, and ITS. While ITP and ITA form stable zincblende solid solutions for all alloy compositions, zincblende ITS is stable only for a range of x less than 0.15. ITP and ITA have considerably larger cohesive energies and elastic constants than does MCT, indicating that they are structurally robust. At a 0.1-eV gap, the band structures near the gap and the electron mobilities in ITP, ITA, and ITS are also found to be comparable to those of MCT. Because the lattice constants of ITP and ITA are less than 2% larger than the respective values in InP and InAs, the latter should provide natural substrates for the growth of active LWIR alloys.

14. SUBJECT TERMS

Metals and alloys, long-wave infrared detectors, electron transport properties

15. NUMBER OF PAGES

16. PRICE CODE

17. SECURITY CLASSIFICATION OF REPORT	18. SECURITY CLASSIFICATION OF THIS PAGE	19. SECURITY CLASSIFICATION OF ABSTRACT	20. LIMITATION OF ABSTRACT
Unclassified	Unclassified	Unclassified	Unlimited

CONTENTS

1. SUMMARY 1

2. TRANSPORT 3

2.1 Introduction 3

2.2 Band Structure 3

2.3 Fermi Level 4

2.4 Hall Coefficient 6

2.5 Drift Mobility 8

2.6 Conclusions 8

3. TEMPERATURE—DEPENDENT BAND GAP 13

4. PHASE DIAGRAMS AND MELTING TEMPERATURES 16

5. DEFECT STUDIES 22

6. INTERACTIONS WITH EXPERIMENTAL GROUPS 24

REFERENCES 25

APPENDICES

A InTIP—A Proposed Infrared Detector Material A-1

B InTIP—A Proposed Infrared Detector Material B-1

C Temperature Dependence of Band Gaps in HgCdTe and Other Semiconductors C-1

D Theoretical Evaluation of InTIP, InTIAs, and InTISb as Long-wave Infrared Detectors D-1

E Letter to Professor Razeghi E-1

FIGURES

1 Electronic structure of $In_{0.92}Tl_{0.08}Sb$ 5

2 Fermi energy as a function of temperature 7

3 Hall factor as a function of temperature 9

4 Mobility as a function of temperature in $In_{0.92}Tl_{0.08}Sb$ 10

5 Mobility as function of temperature 11

6 Change in the gap with temperature 14

7 Test of the Lindemann melting criterion 17

8 Melting temperature vs. transverse optical phonon wave number 18

1. SUMMARY

Researchers at SRI International have calculated properties of $In_{1-x}Tl_xSb$ alloys related to their use as long-wave infrared (LWIR) detectors. Under the contract, we were to look into aspects of native point defects, temperature dependence of band structures, and transport properties. In addition, we were tasked to consult with groups attempting to grow the material. Prior to the actual start of the program, we suggested that the alloys $In_{1-x}Tl_xAs$ and $In_{1-x}Tl_xP$ might also be suitable IR detector candidate materials. Consequently, although we were not tasked to do so, where it proved to be feasible and we had developed general computational methods that could also be used on those materials, we evaluated the corresponding properties of three alloys $In_{1-x}Tl_xX$ with X either, P, As, or Sb (denoted as ITP, ITA, and ITS, respectively).

Some of our major results are summarized in Table 1, where many materials characteristics important to performance of LWIR detectors are presented for the Tl-bearing alloys, along with those of $Hg_{0.78}Cd_{0.22}Te$ (MCT) for comparison. Our theoretical numbers and the corresponding experimentally measured values are included for the HgCdTe alloy to allow us to examine the trustworthiness of the predictions. As can be seen from Table 1, our theories replicate most experimental results in HgCdTe to within 20% or so, and in some cases (e.g., bond lengths) within a few percent. A more extensive comparison between our theory and experiments for a wider range of materials can be found in Table 1 of our contribution to *Applied Physics Letters*, reproduced as Appendix A. The results in Table 1 for $In_{0.33}TlP$ and $In_{0.85}Tl_{0.15}As$ are summarized in Appendix B.

$In_{0.9}Tl_{0.1}Sb$ differs from the other alloys in that its gap, like InSb, closes as temperature increases. At 200 K the gap narrows to ~ 0.05 eV. This sharp variation can cause problems with the spatial uniformity of an array if there are temperature gradients. However, this narrowing also causes the effective mass to decrease, so the electron mobility stays high at the elevated temperature. This should cause the responsivity to remain high and the noise low. The hole effective mass is also lower than that of the other alloys, and this should be reflected in higher hole mobilities and a longer electron Auger recombination time in p-type material. Our results thus indicate that, if the materials can be prepared, high-performance detectors should result.

In addition to the Table 1 results related to LWIR detectors, we have developed some general techniques that enable us to calculate the temperature variations of band structures and the transport properties of any narrow-band-gap material (see Appendix C). We have also found a way to estimate melting temperatures, and have nearly finished a new program enabling rapid accurate determination of defect formation energies.

We have published or submitted four papers on our findings this year; two are major contributions, and two are extensions published in connection with conference proceedings. The papers are Appendices A through D of this report. The paper we presented at the IRIS Materials Specialty Conference (Appendix B) was given the best paper award, which will be presented at the 1995 meeting. In 1995 we will also make two verbal presentations at the 20 to 24 March

Table 1

LWIR MCT ITP, ITA, AND ITS PROPERTIES COMPARISONS

Property		$Hg_{0.78}Cd_{0.22}Te$		$In_{0.33}Tl_{0.67}P$	$In_{0.85}Tl_{0.15}As$	$In_{0.9}Tl_{0.1}Sb$
		Theory	Experiment	Theory	Theory	Theory
1	$\overline{E}_g$ [eV]	0.1	0.1	0.1	0.1	0.1
2	$\overline{E}_b$ [eV/atom]	1.66	1.75	2.75	3.09	3.01
3	$\overline{a}$ [Å]	6.45	6.46	5.92	6.08	6.46
4	$\hbar\omega_{To}$ [meV]	14.5	14.12	34.6	25.8	21.
5	B[10^{12}erg/cm^3]	0.46	0.42	0.61	0.58	0.44
6a	dE_g/dx [eV] @ E_g (77 K) = 0.1 [eV]	1.71	1.69 @ 0 K	1.42	1.80	1.82
6b	dE_g/dT [meV/K]	0.36	0.3	~-0.05	-0.25	-0.25
7	m_e^* @ 0 K	0.008	~0.009	0.008	0.007	0.007
8	m_h^* @ 0 K	0.65	0.38-0.71	0.37	0.375	0.250
9	μ_e[cm^2/V-s]					
9a	@ 80 K	$1.07x10^5$	$0.986x10^5$	$6x10^4$	$1.16x10^5$	$8x10^4$
9b	@ 200 K	$2.24x10^4$	$2.0x10^4$	$4.5x10^4$	$6.72x10^4$	$1.4x10^5$

APS Solid State Physics meeting in San Jose, and an invited talk at the 6 to 10 February SPIE meeting, also in San Jose.

Section 2 discusses our additions to transport theory. Section 3 is devoted to the temperature variation of band gaps. Our progress in estimating melting temperatures, and other quantities related to phase diagrams, is discussed in Section 4. The new technique we are developing to calculate defect formation energies is summarized in Section 5, and additional details of our results can be found in the appendices. Our interaction with experimental groups attempting to grow this material is summarized in Section 6.

2. TRANSPORT

The transport-related properties such as electron mobility, Hall coefficient, and Fermi levels are calculated with accurate analytical band structures, Fermi-Dirac (FD) statistics, and experimental energy gap. Thus, calculated values differ substantially from the ones obtained with effective mass or parabolic band structure approximation of $In_{0.92}Tl_{0.08}Sb$ alloy. We find that approximating the Hall factor by unity over a wide range of temperatures is accurate only for high carrier concentrations. An error of about 20% is expected at low carrier concentration (10^{15} cm^{-3}). The impurity, phonon, and alloy disorder-limited mobility calculations with full solution to Boltzmann transport equation with FD statistics predict a hump near 40 K. Such a hump has been observed in HgCdTe IR alloy. The mobility in $In_{0.92}Tl_{0.08}Sb$ is about 10 to 20% higher than that in HgCdTe.

2.1 INTRODUCTION

The experimental results on electron transport properties of semiconductors is often compared to theory that rests on three approximations, namely, parabolic band structures for those states occupied in the measurement, Maxwell-Boltzmann (MB) statistics, and collision time approximation to the full Boltzmann gain-loss equation. These approximations are made to all scattering mechanisms whether they are elastic or inelastic. It is well known that, even in large-gap materials, the constant effective mass approximation is valid only very near ($\approx E_g/10$) to the band edge (Kane, 1957; Krishnamurthy et al., 1987). This approximation has been recognized to be particularly poor for narrow-gap materials, and nonparabolic corrections calculated in the $k \cdot p$ formalism are often used (Schmidt, 1970; Meyer and Bartoli, 1982; Bartoli et al., 1982). This correction is substantial but still differs considerably from our more accurately calculated band structures. In addition, our fit of the conduction band to an analytical function makes many results transparent and simplifies the calculations. As the Fermi energy can easily move into the conduction band of lightly doped small-gap materials, the form of the Boltzmann equation with FD (instead of the usual MB) statistics must be used to obtain accurate transport coefficients.

Here we report results from our study of absorption coefficient, Fermi energy, Hall coefficient, and electron mobility calculated with FD statistics and accurate pseudopotential band structures fine tuned with tight-binding (TB) corrections.

2.2 BAND STRUCTURE

Quantitatively accurate band structures of group IV elements (Krishnamurthy et al., 1986), III-V compounds (Chen and Sher, 1981), and II-VI compounds (Chen and Sher, 1981; Berding et al., 1987) can be obtained using a minimum set of sp^3 orbitals in semiempirical calculations. First, empirical pseudopotential form factors are used to calculate a TB Hamiltonian H in the minimum set. H is then transformed into a zeroth-order H_0 in an

orthonormal basis. Then, a perturbative Hamiltonian having a first-neighbor TB form is added to H_0 to fine tune the band structure. Because long-range interactions are included in this Hamiltonian, the measured band curvatures are correctly reproduced. This procedure is followed for both InSb and TlSb and then the alloy band structures are calculated in the virtual crystal approximation. Coherent potential approximations are unnecessary because of the very small Tl content.

We focus on $In_{0.92}Tl_{0.08}Sb$ alloy with 100-meV band gap for the studies reported here. We find that the calculated conduction band is replicated very well by a hyperbola,

$$E_k = \left(bk^2 + c^2\right)^{1/2} - c, \tag{1}$$

where b and c are adjusted to fit the calculated band structure in the energy range of interest. When b and c are treated as constants related to the band gap E_g and the effective mass, this expression reduces to the same nonparabolic correction form obtained in the **k·p** method. Our values of b and c are 65.94 and 0.058, respectively, whereas the corresponding **k·p** values are 46.0 and 0.05. The differences are found to be large enough to cause a noticeable change in the band structure. In Figure 1, we show the band structure calculated by diagonalizing the Hamiltonian (thick line), our hyperbolic fit (thin line) **k·p** band structure (thin dotted line) and the effective mass band structures (thick dotted line). We find that our hyperbola fits the band structure calculated by diagonalizing the Hamiltonian quite well up to an energy of 0.6 eV from the conduction band edge. Without loss of accuracy, in the studies considered here, Eq. 1 is used as the energy dispersion relation in transport expressions that follow.

For energies $E-E_c$ greater than 50 meV where the shape of the conduction band is nearly linear in k, the group velocity is a constant independent of the k. Then the density of states (DOS) increases proportional to E rather than $E^{1/2}$ as in the case of parabolic bands. Clearly, these features modify the transport properties of electrons occupying these states. As we will show in the following section, at the carrier concentration and temperatures often found in device structures, the Fermi level falls into the region where these features contribute.

2.3 FERMI LEVEL

The calculation of Fermi level ε_F as a function temperature T and doping concentration n_D is required for all transport calculations. A knowledge of temperature-dependent gap $E_g(T)$ is essential to obtain ε_F. Ideally, temperature dependence should be included in the Hamiltonian from which the variation of E_g with T could be obtained. We have developed a general method to incorporate phonon effects on the band gap. However, we have used the experimental values (Sher et al., 1986) of the gap.

The ε_F is calculated from the condition (Sze, 1981) that at a given T the number of electrons in the conduction band is the sum of electrons excited from the valence band and donor levels. In this study where the modifications caused by the band structures are being emphasized, the donor states are assumed to be located at the bottom of the conduction band. The valence and conduction band DOS are calculated from our band structure. The valence band

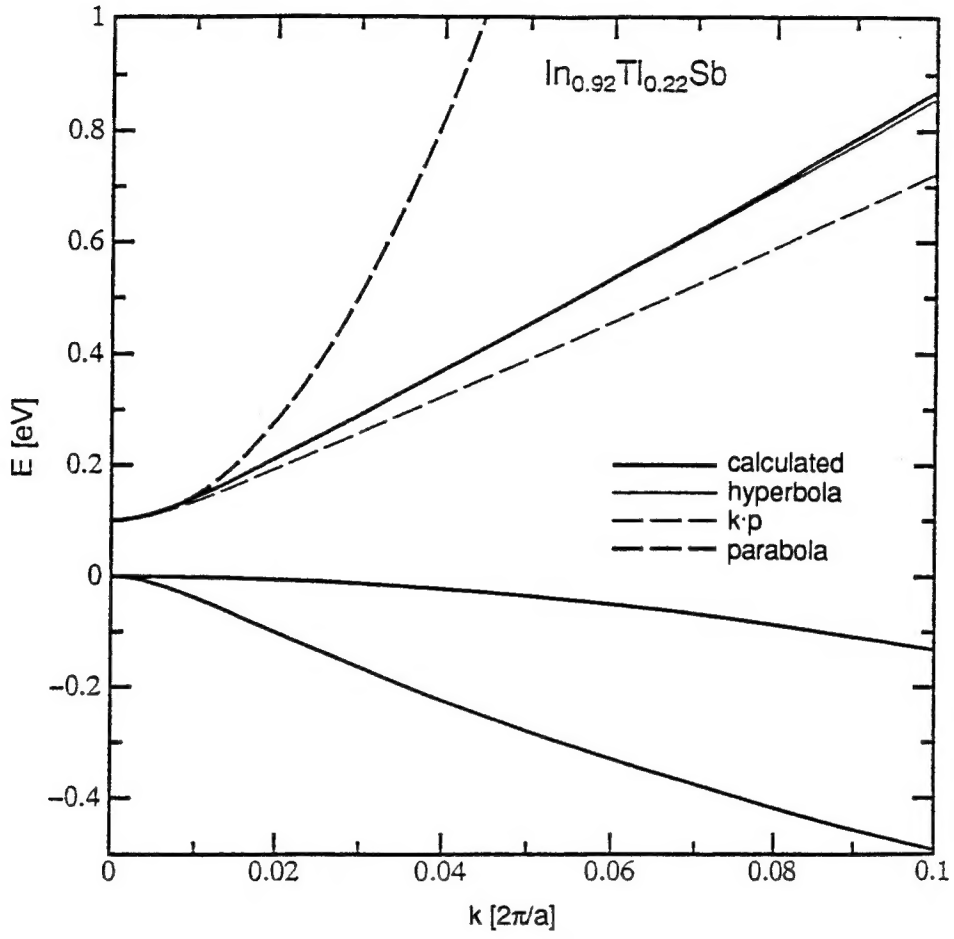

Figure 1

Electronic Structure of $In_{0.92}Tl_{0.08}Sb$.
The crystal momentum k is in units of 2 π/a where a is the lattice constant.

DOS yields a hole effective mass of 0.25. The ε_F (measured from valence band edge) as a function of T and n_D calculated from hyperbolic band structures are given in Figure 2.

2.4 HALL COEFFICIENT

The carrier density, n in n-type material, is normally deduced from measurements of Hall coefficient R_H, given by r_e/en, by assuming the Hall factor r_e is unity. If one uses parabolic approximation and MB statistics, r_e is approximately unity. Examining the effect of removing these approximations, using the correct band structures, requires generalizing the Boltzmann transport equation (BTE) to include FD distribution function. We have

$$\frac{df(\mathbf{k})}{dt} = \sum_{\mathbf{k}'}\left[w(\mathbf{k},\mathbf{k}')f(\mathbf{k}')(1-f(\mathbf{k})) - w(\mathbf{k}',\mathbf{k})f(\mathbf{k})(1-f(\mathbf{k}'))\right]. \tag{2}$$

The first term of the right side of Eq. 2 is the gain term, and the second term is the loss term. In equilibrium, the left side is identically zero, and f becomes the equilibrium FD distribution function f_0, given by

$$f_0(E_{\mathbf{k}}) = \left(e^{\beta(E_{\mathbf{k}}-\varepsilon_F)}+1\right)^{-1}, \tag{3}$$

where β is $(k_B T)^{-1}$. In the presence of electric and magnetic fields,

$$\frac{df(\mathbf{k})}{dt} = \frac{\partial f(\mathbf{k})}{\partial t} + \nabla f(\mathbf{k})\cdot\frac{e}{\hbar}(\mathbf{E}+\mathbf{v}\times\mathbf{B}). \tag{4}$$

In steady state, the $\partial f(\mathbf{k})/\partial t$ in Eq. 4 vanishes. In the small field regime, we can linearize f and write it as a sum of f_0 and a perturbation $f_1(\mathbf{k})$. Disregarding the derivative of $f_1(\mathbf{k})$ and after some algebraic manipulation, Eq. 4 reduces to

$$\nabla f_0(\mathbf{k})\cdot\frac{e}{\hbar}(\mathbf{E}+\mathbf{v}\times\mathbf{B}) = \sum_{\mathbf{k}'}\left[W(\mathbf{k},\mathbf{k}')f_1(\mathbf{k}') - W(\mathbf{k}',\mathbf{k})f_1(\mathbf{k})\right], \tag{5}$$

where the renormalized W and the usual transition probability per unit time w are related by

$$W(\mathbf{k},\mathbf{k}') = w(\mathbf{k},\mathbf{k}')\frac{(1-f_0(\mathbf{k}))}{(1-f_0(\mathbf{k}'))}. \tag{6}$$

Note that for elastic scattering W and w are equal. However, for inelastic cases the effect depends on whether energies at $\mathbf{k}$ and $\mathbf{k}'$ are larger or smaller than ε_F. If both initial and final energies are larger (or smaller) than ε_F, only a small correction to w is expected. However, if the initial state is above ε_F and the final state is below ε_F, that scattering is suppressed.

In the collision time approximation, the gain term in Eq. 6 is neglected and the effective collision time τ_k^F is

$$\left(\tau_k^F\right)^{-1} = \sum_{\mathbf{k}'} W(\mathbf{k}',\mathbf{k}). \tag{7}$$

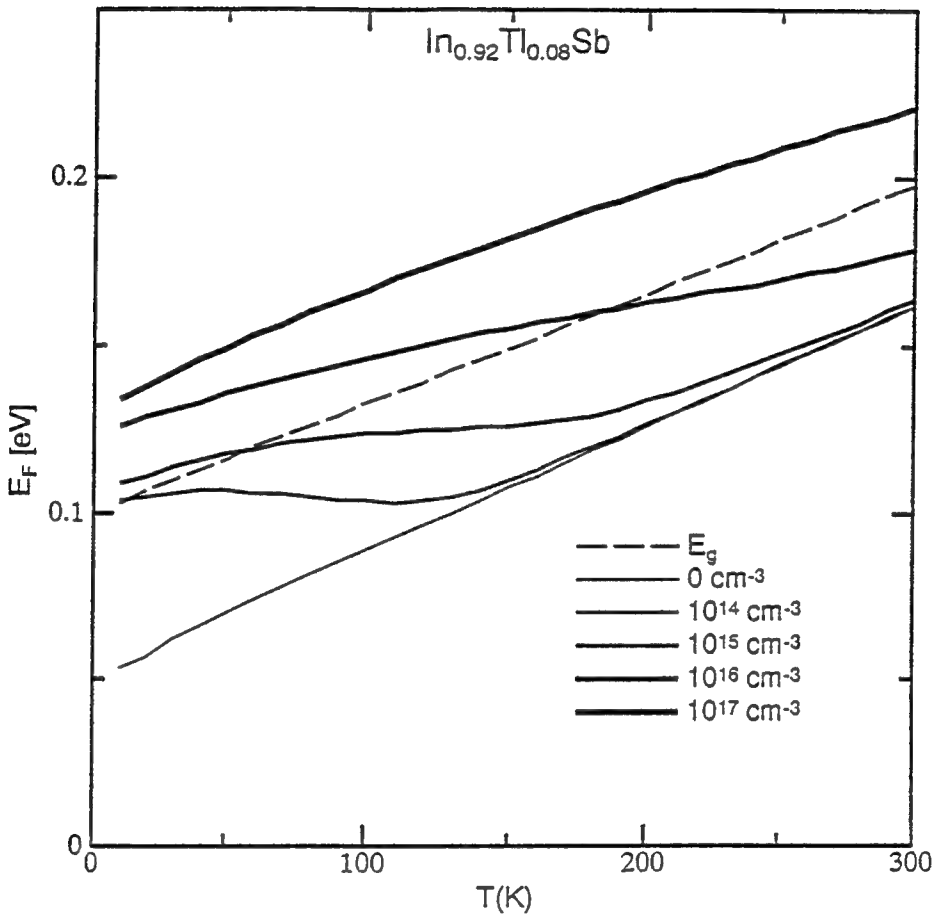

Figure 2

Fermi Energy as a Function of Temperature

Using this collision time approximation, it is straightforward to obtain the expression for r_e:

$$r_e = 3k_B T\left[\frac{(\Sigma_k f_0)\Sigma_k k^2\gamma_k^3(\tau_k^F)^2 f_0(1-f_0)}{\left(\Sigma_k k^2\gamma_k^2\tau_k^F f_0(1-f_0)\right)^2}\right], \tag{8}$$

where γ_k is defined $\nabla_k E_k \equiv \gamma_k k$. The values of r_e calculated with hyperbolic bands and those obtained with parabolic bands differ substantially. The calculated r_e with hyperbolic band structures is shown for various T and doping densities in Figure 3. The r_e is approximately 1 for doping concentrations of 10^{16} cm^{-3} or higher. However, at lower doping concentrations, r_e shows considerable structure with values differing by ±20%. The experimentalists normally use a value of 1 for r_e in deducing the intrinsic density from Hall measurements, suggesting that reported values may be smaller by as much as 20% at low concentrations.

2.5 DRIFT MOBILITY

The formalism developed above to find the solution to BTE with FD statistics can be used to calculate the mobility μ. We obtain the following expression in collision time approximation:

$$\mu = \frac{e}{3\hbar^2 k_B T}\left[\frac{\Sigma_k k^2\gamma_k^2\tau_k^F f_0(1-f_0)}{\Sigma_k f_0}\right]. \tag{9}$$

The mobility calculated by including the scattering due to ionized impurities and polar optic phonons as a function of temperature and doping density is shown in Figure 4. The change in the Debye screening length, complicated variation of Fermi level, and phonon scattering give rise to a hump in mobility near 150 to 200 K at lower doping concentrations as seen in Figure 4. However, it is well known that the collision time approximation always overestimates the velocity transition rate that determines the mobility. For meaningful comparison with experiment, we generalized the above procedure to get full solution to BTE (Krishnamurthy and Sher, 1993). This calculated mobility with our hyperbolic band structures is compared with that obtained from k·p band structure with collision time approximation in Figure 5 for an impurity concentration of $10^{14}cm^{-3}$. The interesting feature of a hump near 100 K is totally wiped out in this approximation.

One important feature of Figure 5 is that the hump in mobility near 100 K could be explained with competing impurity and phonon scattering rates. A hump in mobility in IR material, HgCdTe, is seen experimentally. We also found that the mobility in HgCdTe is about 30% higher than in $In_{0.92}Tl_{0.08}Sb$ at 77 K.

2.6 CONCLUSIONS

We have studied the effect of various approximations on electron transport coefficients in $In_{0.92}Tl_{0.08}Sb$ and on ways to extract physical parameters from experiments. We point out how the values interpreted from experiments depend crucially on various approximations such as effective mass, MB statistics, and collision time. The main results are the following:

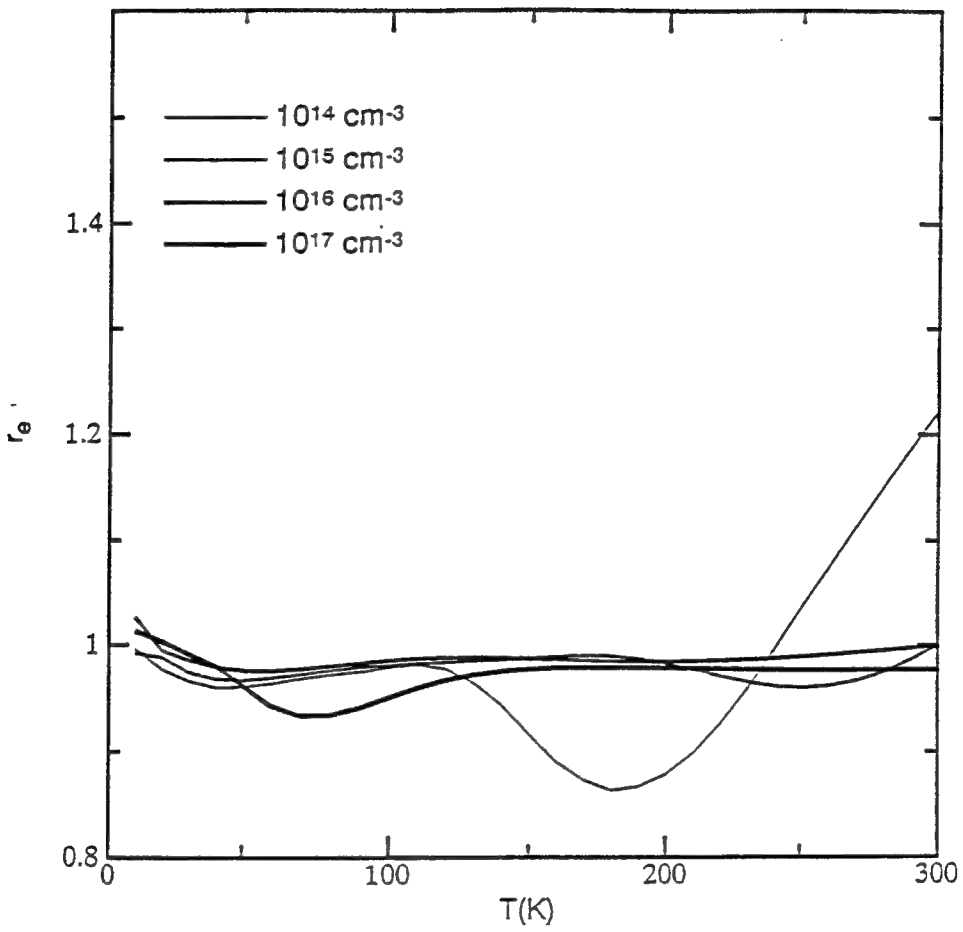

Figure 3

Hall Factor as a Function of Temperature

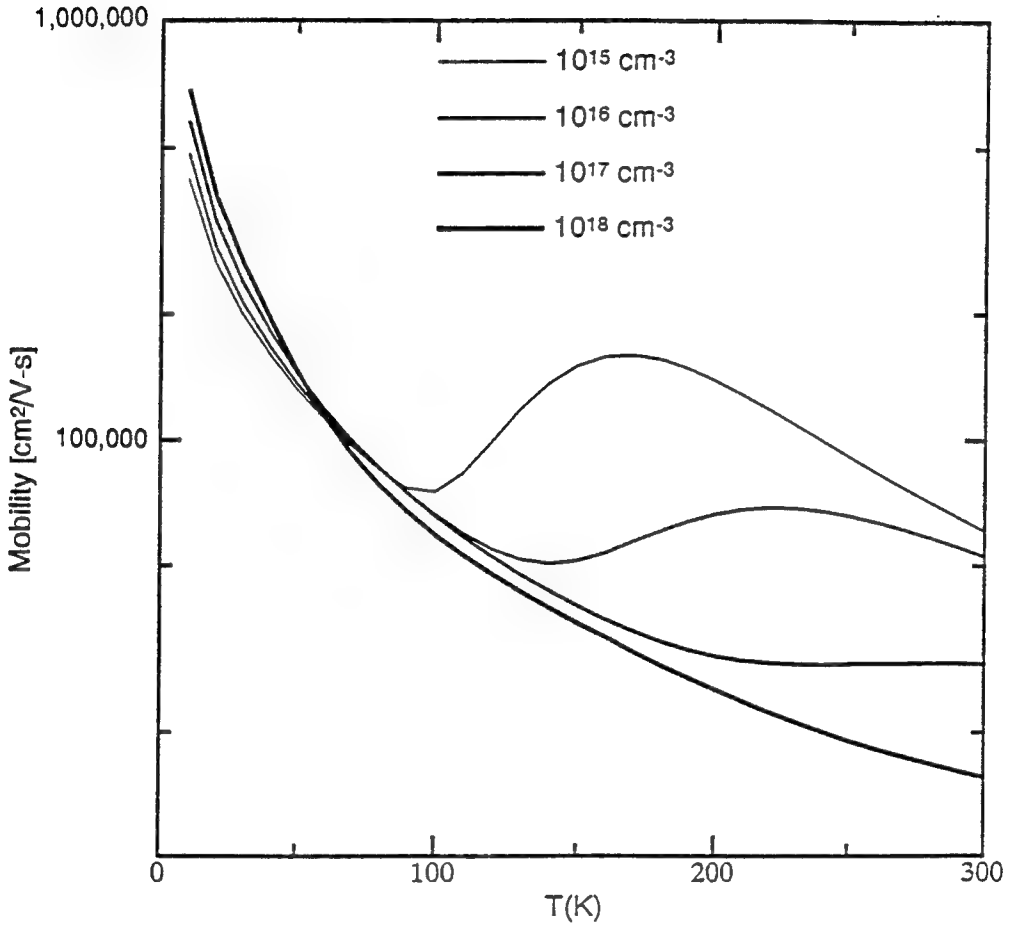

Figure 4

Mobility as a Function of Temperature in $In_{0.92}Tl_{0.08}Sb$

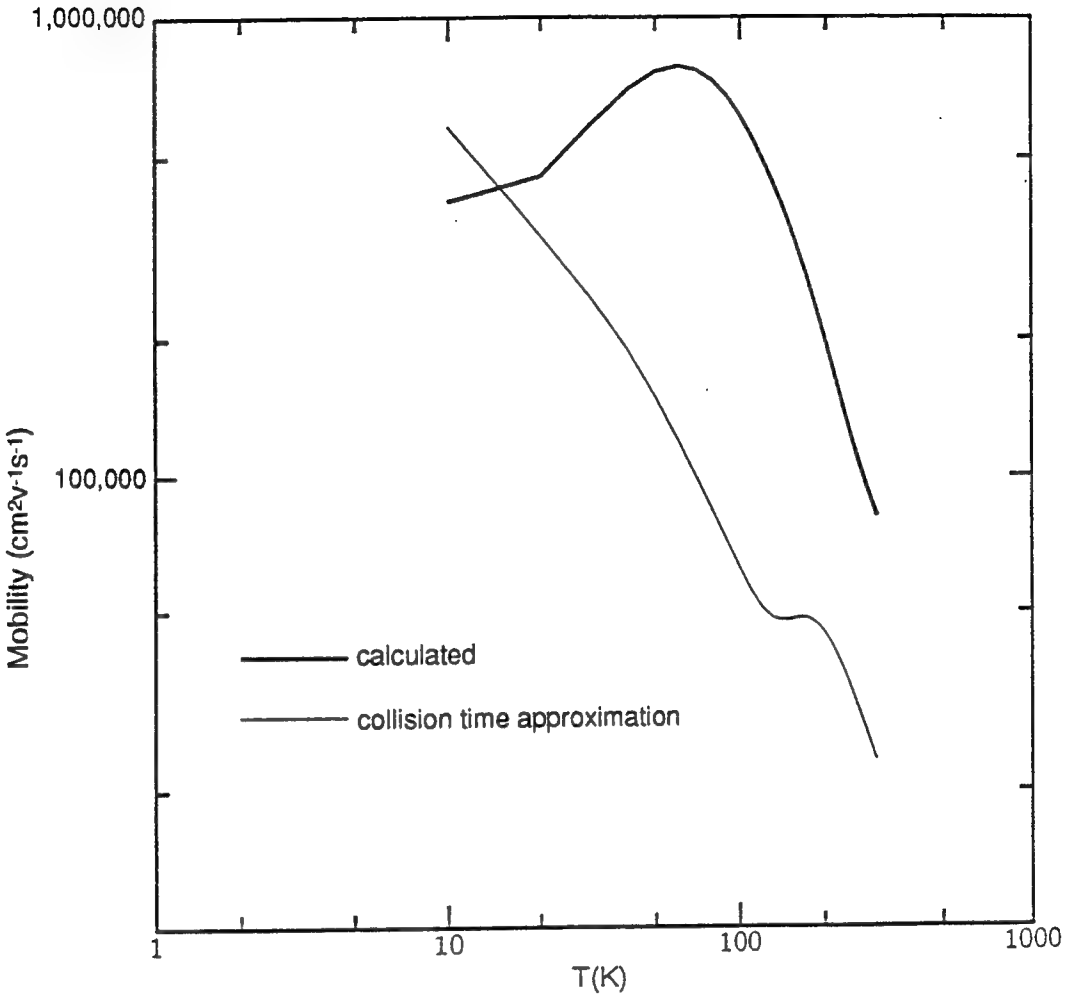

Figure 5

Mobility as a Function of Temperature

- Approximating the Hall factor by unity over a wide range of carrier concentrations is accurate only for low temperatures, typically less than 100 K. An error of about 20% is expected at high temperatures and carrier concentration lower than (10^{15} cm^{-3}).

- The mobility calculations with full solution to BTE with FD statistics predict a hump near 100 K. At the usual operating temperature of 77 K, the mobility in $In_{0.92}Tl_{0.08}Sb$ is about 30% smaller than that in HgCdTe. However, at room temperature, mobility in $In_{0.92}Tl_{0.08}Sb$ is about a factor of 5 higher than that in HgCdTe. It should be noted that when the temperature-dependent band structures are used, the mobility ratio changes substantially, as these two materials behave differently with temperature. This aspect is discussed in following section.

3. TEMPERATURE—DEPENDENT BAND GAP

When the temperature of the lattice is increased, the lattice expands. This expansion, usually called dilation, decreases the band gap. The number of phonons in the lattice increases with temperature. The change in potentials caused by the displacement of atoms from their equilibrium positions introduces an electron-phonon interaction. This interaction, viewed as a perturbation, changes the electronic states, that is, the band structure. A major contribution to the band gap change with temperature arises from this interaction.

The electron-acoustic-phonon interactions are usually parameterized in terms of wave-vector- and energy-independent deformation-potential coupling constants. Our calculations generalized the above approach considerably. We use accurate tight-binding band structures for electrons and the valence force field model for phonon band structures. We include contributions from all six phonon modes, with wave vectors spanning the entire Brillouin Zone.

These calculations require knowledge of spatial dependence of atomic potentials in the bulk. We assume that attractive interatomic matrix elements vary as r^{-m} and the Coulomb repulsive interaction varies as V_0/r^{2m}. The two unknowns, m and V_0, are adjusted so that total energy calculations yield an accurate equilibrium bond length and bulk modulus.

Once the spatial dependence of potentials is known, electron-phonon interactions can be calculated by expanding the potentials in a Taylor's expansion. Because the atomic displacements are small compared to the bond length, only the first two terms are retained. The change in energy state at a given electron wave vector is obtained in a second-order, stationary-state perturbation theory.

Our calculation steps can be summarized as follows: (1) Choose the energy state whose temperature variation needs to be obtained. Get the corresponding electron wave vector, k. (2) Choose a phonon wave vector, q. (3) Calculate the dynamical matrix in the volume force field (VFF) model and diagonalize it to get the atomic displacements for all six modes. (4) From a knowledge of first and second derivatives of the potentials in the local basis, calculate the matrix elements, $\langle k|H_1|k\rangle$ and $|\langle k - q|H_2|k\rangle|^2$. (5) From second-order perturbation theory, obtain the change in energy with temperature. The calculation of energy gap variation requires repeating the above procedure for conduction and valence band edges. Details of these calculations are given in Appendix C.

The results of our calculations carried for InSb and the $In_{0.92}Tl_{0.08}Sb$ alloy are shown in Figure 6. The calculated change in the energy gap of InSb compares extremely well with various experiments. The gap decreases with temperature. As the InSb content is very large in $In_{0.92}Tl_{0.08}Sb$ alloy, the change in the gap merely follows that of InSb. Although $In_{0.92}Tl_{0.08}Sb$ alloy is a narrow-gap IR material, the gap decreases with temperature. At 77 K, the gap reduces by 10 meV. This is in sharp contrast to a well-known IR material, HgCdTe, where the gap increases with temperature. Although the variation is shown up to 750 K, our model predicts

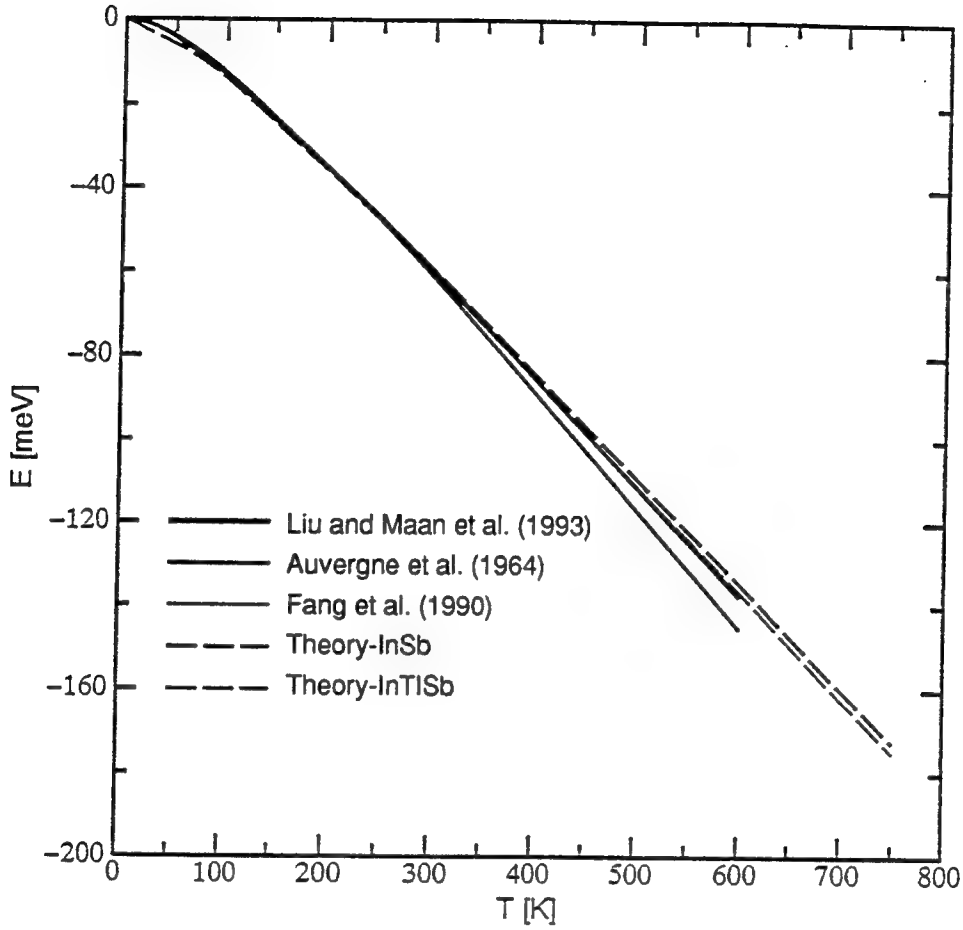

Figure 6

Change in the Gap with Temperature

that the gap closes completely at around 450 K. However, when higher-order terms that include interactions between the valence and conduction bands are used, the gap, albeit very small, may stay open at temperatures below the predicted 450 K closing temperature.

4. PHASE DIAGRAMS AND MELTING TEMPERATURES

We have begun, but not completed, a study to estimate the phase diagrams of InTlP and InTlAs, in a manner similar to what we have done for InTlSb (Chen et al., 1993). The first task is to estimate the melting temperatures for the Tl binaries. According to the Lindemann melting criterion, the r.m.s. bond-length fluctuations ζ at the melting temperature T_m is a proportional constant. ζ can be estimated from the equipartition theorem $<M\omega^2 \zeta^2>=kT_m$, where M is the reduced mass $M=M_AM_C/(M_A+M_C)$ with M_A and M_C being, respectively, the masses of the anion and cation in the compound, ω the transverse phonon frequency, and k the Boltzmann constant. Combining these two results, we obtain $T_m=CM\omega^2a^2$, where C is another constant. Table 2 lists the quantities entering $M\omega^2a^2$ and its values. These entry values for the Tl compounds were calculated by van Schilfgaarde et al. (1994), as reproduced in Appendix A, while those for the other systems are the empirical values (Chen and Sher, 1995). The results show that this simple theory does not work for these systems. To explicitly show this, T_m is plotted as a function of the product $M\omega^2a^2$ in Figure 7, illustrating that T_m is not at all proportional to $M\omega^2a^2$.

On the other hand, when plotted against ω for the systems with the same anion, T_m exhibits a smooth function, as shown in Figures 8a through 8c. A simple quadratic extrapolation can be made to obtain an estimate of T_m for the Tl compounds. These are the values listed in Table 2 for the Tl compounds.

Our next step is to extrapolate the mixing enthalpies Ω and entropies of fusion ΔS for the binary systems. From the values listed in Table 2, no simple extrapolation is seen to be reliable, because the variations are large and irregular. Those numbers listed in Table 2 for the Tl compounds are the guessed values. Although these values will not give a quantitative prediction of the phase diagrams on InTlP and InTlAs, we can predict that the phase diagrams of these two alloys will behave like those of the common III-V alloys (Chen and Sher, 1995). Unlike InTlSb, which has a complicated phase diagram (Chen et al., 1993) due to the existence of a stable CsCl structural phase for pure TlSb, both InTlP and InTlAs are expected to be grown in the zincblende structure from liquid-phase epitaxy (LPE) and the bulk growth method. A more quantitative theoretical prediction of the growth conditions, however, requires a more rigorous calculation combining local density approximation (LDA) and Monte Carlo simulations.

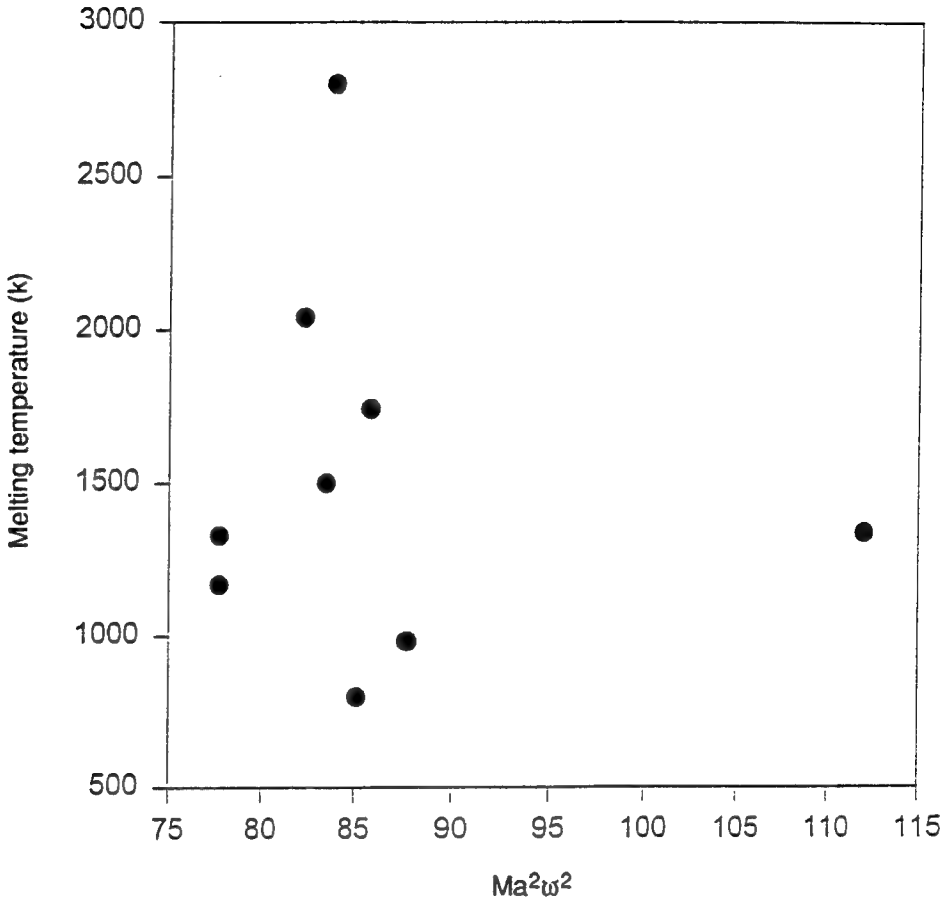

Figure 7

Test of the Lindemann Melting Criterion

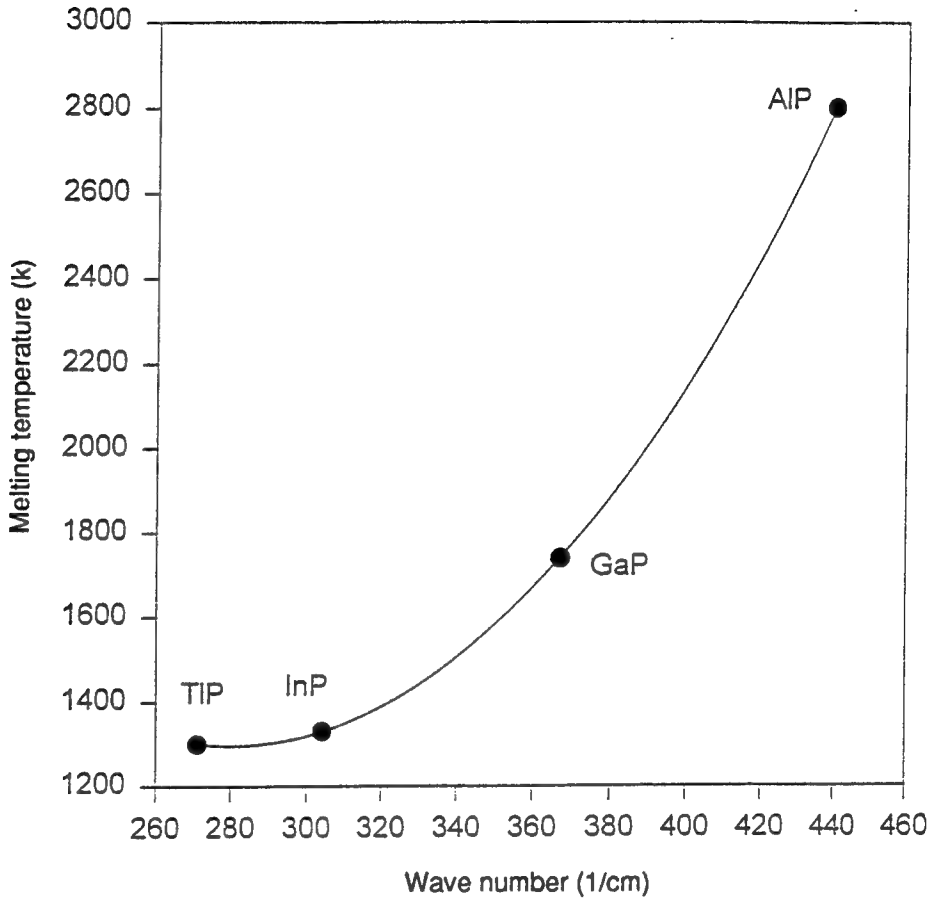

(a) XP Semiconductors with X = Al, Ga, In, Tl

Figure 8

Melting Temperature vs. Transverse Optical Phonon Wave Number

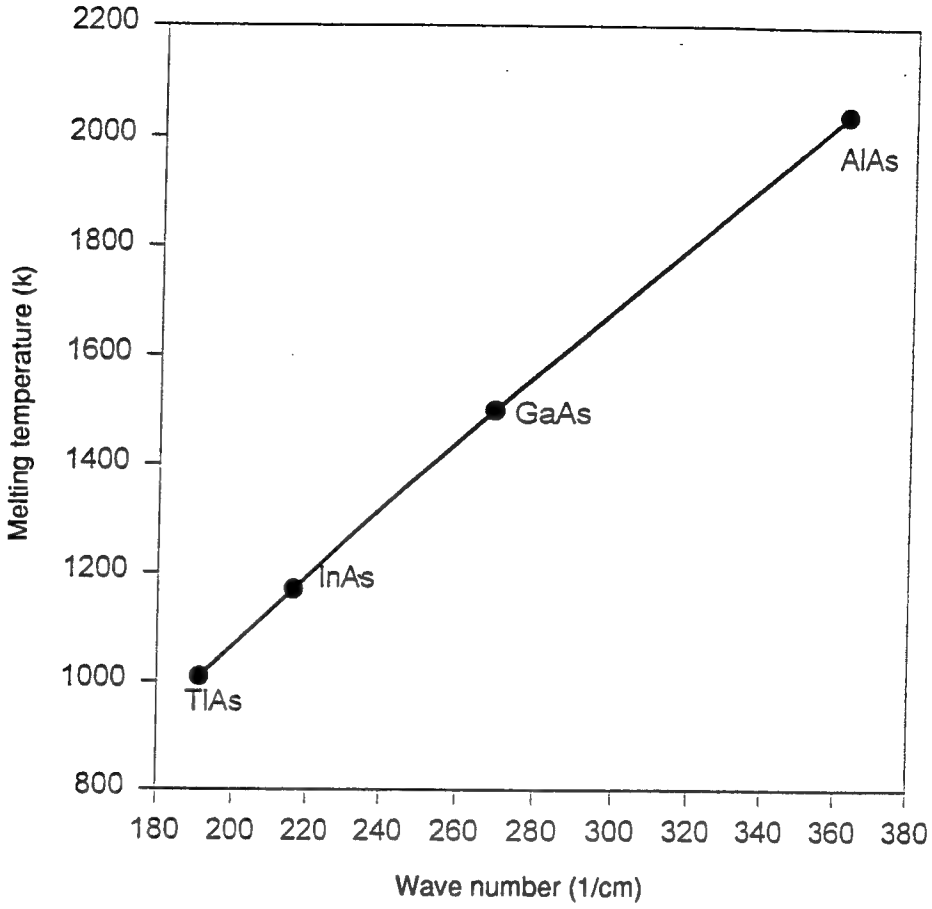

(b) XAs Semiconductors with X = Al, Ga, In, Tl

Figure 8

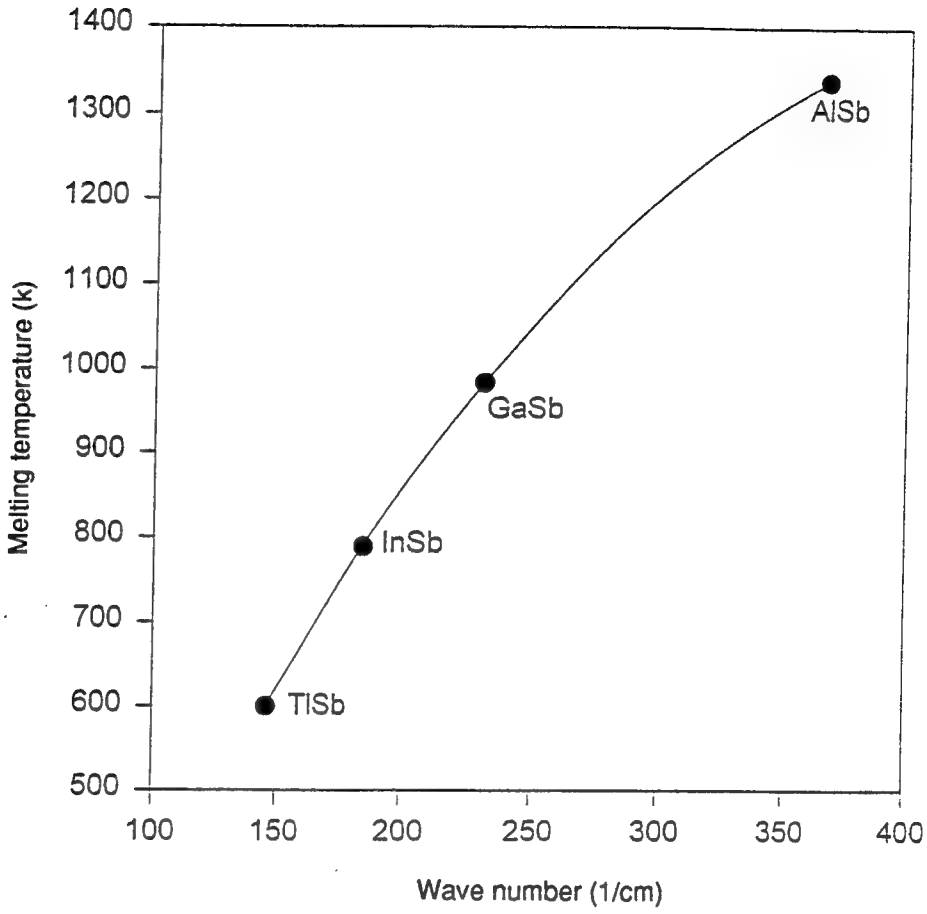

(c) XSb Semiconductors with X = Al, Ga, In, Tl

Figure 8

Table 2

VALUES OF THE LATTICE CONSTANT a (IN Å), THE ZONE-CENTER TRANSVERSE OPTICAL PHONON FREQUENCY ω (IN TERMS OF THE CORRESPONDING WAVE NUMBER IN 1/CM), THE REDUCED MASS M (IN μ), THE MELTING TEMPERATURE T_M (IN K), THE BINARY MIXING ENTHALPY PARAMETER ω (IN CAL. PER MOLE) IN BINARY LIQUID, AND THE ENTROPY OF FUSION ΔS (CAL/K) FOR III-V COMPOUNDS. EXCEPT FOR THE TL COMPOUNDS, ALL THE ENTRIES ARE TAKEN FROM CHEN AND SHER (1995). THE VALUES OF a AND ω FOR THE TL COMPOUNDS ARE THE CALCULATED VALUES FROM VAN SCHILFGAARDE ET AL. (1994), AND THOSE INSIDE THE PARENTHESES ARE THE ESTIMATED VALUES.

System	a	ω	M	T_m	$10^{-6}M\omega^2a^2$	Ω	ΔS
AlP	5.47	440	14.41	2800	83.5	2800–4.8T	15.7
GaP	5.45	367	21.43	1740	85.7	28000–4.8T	16.8
InP	5.87	304	24.37	1330	77.6	4500–4.0T	14.0
TlP	5.96	271	26.86	(1300)	(70.1)	(4000–4.0T)	(13.0)
AlAs	5.64	361	19.84	2040	82.2	600–12T	15.6
GaAs	5.65	269	36.12	1500	83.4	5160–9.16T	16.64
InAs	6.06	216	45.34	1179	77.7	3860–10T	14.52
TlAs	6.18	191	54.82	(1010)	(76.4)	(3500–10T)	(13.5)
AlSb	6.14	366	22.09	1338	111.5	1230–10T	14.74
GaSb	6.09	231	44.34	983	87.7	4700–6T	15.8
InSb	6.49	185	59.09	798	85.2	3400–12T	14.3
TlSb	6.59	146	76.30	(600)	(70.6)	(3000–12T)	(13.3)

5. DEFECT STUDIES

The materials issues surrounding growth of $In_{1-x}Tl_xX$ alloys are evidently complex and complicated by a dearth of information in the early stages of attempting to synthesize a new material. One of the most serious impediments to a theoretical study of the In-Tl-X ternary is the lack of geometrical information. Thus, most likely crystal structures for different compositions of Tl, In and X must be assumed or obtained from the theory. Another impediment is the need for accurate determination of the energetics of molecular species, as well as the bulk crystal energies, in that gas phase. These energies, together with the entropy, are the quantities needed to obtain the free energy of the In-Tl-X ternary. To calculate the native point defect and the impurity substitutional energies, these same methods can be extended to large supercells, each containing a defect (Berding et al., 1994).

To meet these needs, we have invested some effort to extend the capabilites of a new electronic structure method that we developed recently for doing *ab initio* molecular dynamics simulations on molecules of rather large size. This method is highly efficient; moreover, it computes the forces for molecular dynamics simulations. The elements of the method are described briefly below. Several extensions to the program are required to calculate quantities of interest to the In-Tl-X ternary. These include making the program spin-polarized and relativistic, and applying crystalline adaptation of the method for bulk calculations. The first two extensions have been completed, and we now have in hand the energetics of a number of molecular species of interest, including the X_2 and X_4 molecules. An adaptation of a crystalline version of the program is now well under way.

To sketch the elements of the method (Methfessel and van Schilfgaarde, 1993) we first observe that in any method, the main difficulty arises because three elements are necessary: (1) representation of the charge density in some basis and generation of the potential from it, (2) the construction of matrix elements of the Hamiltonian, and (3) the generation of an output density by summing over the square of the calculated eigenvectors. All are more or less trivial when a plane-wave basis is used to represent both the charge density and the basis, but there is generally no convenient analytical representation of wave function products. Our new method approximates a product of two functions centered on separate sites as a linear combination of smoothed Hankel functions centered on these sites (Methfessel and van Schilfgaarde, 1993).[1] This approximation is done once and for all by a least-squares fit of basis function products as a function of internuclear spacing, so that mapping a product of two functions amounts essentially to a table lookup, followed by rotation matrices to a general orientation. As with plane-wave representations, the error in the approximation can be made arbitrarily small by increasing the

[1] Smoothed Hankels are used as the fitting functions because solution of Poisson's equation is analytic, making Step 1 simple. Smoothed Hankel functions were invented by Methfessel, and reduce to ordinary Hankels or Gaussians in limiting cases.

number of functions that approximate a product. The key advantage to this representation is that all functions are atom-centered Hankel and strictly local: they do not extend over all space as do plane waves. While they are more complicated to work with, potential gains in efficiency more than compensate for the added complexity.

For structural relaxation and molecular dynamics of host crystals, surfaces, and defects, uniform, internuclear forces are essential.[2] Customarily, they are calculated by the Helman-Feynman theorem, which uses the property that, at self-consistency, the total energy is stationary to first order with respect to changes in the electron density. A large drawback to the Helman-Feynman approach is that forces are stationary only to zeroth order, since one order of convergence is "used up" in the theorem. This means that forces converge more slowly than the total energy in iterations toward self-consistency. A second error arises when a minimal basis is used, because the basis moves with virtual displacements of the nuclei. A new force theorem we recently developed simultaneously overcomes both problems by allowing the charge density to shift rigidly with nuclear displacements. We can do so because the density is decomposed as a superposition of atom-centered functions. Thus, we obtain additional terms, and the resulting expression is in fact an essentially exact differentiation of the functional we use. In practice, the forces in our method converge as quickly as does the total energy, showing that the rigid shift makes a significant improvement over the Helman-Feynman theorem.

We elected to spend our time on this segment finishing the general program, rather than just calculating the defects in InSb by using our current method (Berding et al., 1994) as called out in the task list (Task 1). Once the new method is completed, a number of materials can be investigated with little effort. Unfortunately, this program development has taken longer than anticipated. It should be completed in a month or so, at which time we will publish results for all the alloys of interest in this development, including InSb.

---

[2] Classical schemes, such as the embedded atom method, employ an *ad hoc* construction of an interatomic potential, and fit-free parameters of the assumed form to selected experimental data. Here the forces emerge explicitly as a byproduct of the LDA.

6. INTERACTIONS WITH EXPERIMENTAL GROUPS

We have talked to several groups who contemplated growing InTlSb alloys by a variety of means. These included groups at Northwestern University headed by Professor Razeghi, at Spire Corporation, and at SRI headed by Dr. A. Sanjuro. The only one that we know produced material this year was the Northwestern group. The SRI group was unfunded and consequently made no progress, and the Spire researchers asked for advice, but we did not receive anything back from them. The Northwestern group sent us a copy of a thesis early in 1994. A copy of the letter we sent in response is in Appendix E. Several aspects of their results puzzled us. We suggested alternative explanations for their observations and modifications to their growth procedure intended to improve their material. While Professor Razeghi in several telephone conversations offered to send us additional data, we did not receive anything.

REFERENCES

Auvergne, A., J. Camassel, H. Mathieu, and M. Cardona (1964), *Phys. Rev.*, B9, 5168.

Bartoli, F.J., J.R. Meyer, R.E. Allen, and C.A. Hoffman (1982), *J. Vac. Sci. Technol.*, 21, 241.

Berding, M.A., M. van Schilfgaarde, and A. Sher (1994), "First-Principles Calculation of Native Defect Densities in $Hg_{0.8}Cd_{0.2}Te$," *Phys. Rev.*, B15, 50, 1519.

Berding, M.A., S. Krishnamurthy, A. Sher, and A.-B. Chen (1987), *J. Vac. Sci. Technol.*, A5, 3014.

Chen, A.-B., and A. Sher (1981), *Phys. Rev.*, B23, 5360.

Chen, A.-B., and A. Sher, "Semiconductor Alloys–Physics and Materials Engineering," to be published book by Plenum Press, 1995.

Chen, A.-B., M. van Schilfgaarde, and A. Sher (1993), "Comparison of In1-xTlxSb and Hg1-xCdxTe as Long Wavelength Infrared Materials," *J. Electronics Materials*, 22, 843.

Fang, Z.M., K.Y. Ma, D.H. Jaw, R.M. Cohen, and G.B. Stringfellow (1990), *J. Appl. Phys.*, 67, 7034.

Kane, E.O. (1957), *J. Phys. Chem.*, Solids 1, 249.

Krishnamurthy, S., A. Sher, and A.-B. Chen (1986), *Phys. Rev.*, B33, 1026.

Krishnamurthy, S., A. Sher, and A.-B. Chen (1987), *J. Appl. Phys.*, 61, 1475.

Krishnamurthy, S., and A. Sher (1993), *J. Appl. Phys.*, 75, 7904.

Liu, P.Y., and J.C. Maan (1993), *Phys. Rev.*, B47, 16274.

M. Methfessel and M. van Schilfgaarde (1993), "Derivation of Force Theorems in Density-Functional Theory," *Phys. Rev.*, B48, 4937.

Meyer, J.R., and F.J. Bartoli (1982), *J. Vac. Sci. Technol.*, 21, 237.

Schmidt, J.L. (1970), *J. Appl. Phys.*, 41, 2876.

Sher, A., D. Eger, A. Zemel, H. Feldstein, and A. Raizman (1986), *J. Vac. Sci. Technol.*, A4, 2024.

Sze, S.M. (1981), *Physics of Semiconductor Devices* (Wiley, New York), p. 22.

van Schilfgaarde, M., A.-B. Chen, S. Krishnamurthy, and A. Sher, "InTlP–A Proposed Infrared Detector Material," *Appl. Phys. Lett.*, in press, 1994.

Appendix A

InTlP—A PROPOSED INFRARED DETECTOR MATERIAL

InTlP — a proposed infrared detector material

M. van Schilfgaarde, An-Ban Chen,[a] S. Krishnamurthy, and Arden Sher
SRI International, Menlo Park, California 94025

(Received 4 March 1994; accepted for publication 23 September 1994)

$In_{1-x}Tl_xP$ is proposed as a promising material for infrared detectors. A number of key optical and structural properties are studied within local density-functional theory. $In_{1-x}Tl_xP$ at $x=0.67$ and $In_{1-x}Tl_xAs$ at $x=0.15$ are estimated to have a gap of 0.1 eV. Their binding energies are larger than that of InSb, and they are found to form stable zinc-blende alloys for all x. $In_{1-x}Tl_xP$ nearly lattice matches to InP, and offers the potential to integrate detector array and read-out circuit. © *1994 American Institute of Physics.*

We propose that the $In_{1-x}Tl_xP$ pseudobinary alloy, grown epitaxially on InP substrates, has the potential of satisfying all the requirements of staring infrared focal plane arrays (FPAs). Currently the leading contenders to support staring FPAs are $Hg_{0.7}Cd_{0.3}Te$, InSb, and Pt:Si for midwave infrared (3–5 μm), and $Hg_{0.78}Cd_{0.22}Te$ for long-wave (8–12 μm). An enormous effort has brought these technologies to a state of maturity where arrays as large as 512×512 pixels can be manufactured with practical yields and at still high but marginally acceptable cost. One major failing of the HgCdTe- and InSb-based FPAs is that the detector array must be In bump-bonded to the read-out integrated circuit (ROIC) on Si substrates, which limits array sizes and stability. Large numbers of native defects also limit performance in HgCdTe arrays. The Pt:Si arrays, while they can potentially be integrated onto the same Si chip that houses the ROIC, have very low quantum efficiency (approximately 1%) which severely limits performance. As future demands are made for still higher signal-to-noise at higher operating temperatures, multispectral responses, larger arrays of small pixels, longer operational life times, and lower production costs, it is not clear that the current materials will be able to satisfy them. Several other materials have been suggested to meet these requirements, including strained layer superlattices, and quantum well infrared photoconductors. They can be built on GaAs substrates, so there is a prospect for their monolithic integration with an ROIC on the same chip. However, both of these devices have low quantum efficiencies (less than 10%) and the quantum wells have awkward optics.

We shall argue, on the basis of first-principles density-functional calculations, that $In_{1-x}Tl_xP$ is rugged, can be grown in the zinc-blende (ZB) structure for all compositions x with its lattice constant nearly matching that of InP, is comparatively free of native point defects, and has the high mobility and infrared absorption needed for high performance devices. We predict that TlP has a negative gap (−0.27 eV) analogous to HgTe (−0.30 eV), and therefore, the gap of $In_{1-x}Tl_xP$ spans the entire IR spectrum. InP is a good electronic material with a functional passivant/insulator (SiO_2), so it can support high performance ROIC devices. Thus, $In_{1-x}Tl_xP$ grown on InP can satisfy all future system requirements. $In_{1-x}Tl_xAs$ is also predicted to be a suitable IR detector. However, InP is a better substrate than InAs, and $In_{1-x}Tl_xP$ offers the advantage of monolithic integration onto an ROIC chip.

Let us assume for the moment that TlP and TlAs can be grown in a zinc-blende structure, and compare some of their key structural properties to those of CdTe and HgTe, as predicted by local density-functional theory. Table I lists some such properties, which were calculated by a full-potential version of the LMTO method.[3] All-electron density functional calculations predict mechanical and structural properties in good agreement with experiment for all known ZB semiconductors,[4] as Table I shows for the compounds listed. Errors in the LDA are small but systematic;[4] because we wish to use the LDA to predict properties of compounds as yet unmade, we make corrections to the LDA to arrive at the predicted values in Table I.

For the cohesive energy we can estimate the LDA errors by including gradient corrections to the local density-functional. The gradient corrections are found to eliminate, and indeed slightly overcorrect for the LDA overbinding in the zinc-blende compounds,[4] as we see in Table I for the known compounds listed. Binding in TlP is comparable to InSb, and far stronger than in HgTe. Also listed are data linearly interpolated for the alloys $In_{0.33}Tl_{0.67}P$, $In_{0.85}Tl_{0.15}As$, and $Hg_{0.78}Cd_{0.22}Te$ (compositions which are predicted to produce a 0.1 eV bandgap, as we discuss later). The relatively large elastic constants are another indication that TlP and TlAs are relatively robust ZB compounds, with a chemical bond and mechanical properties comparable to those of InAs. They suggest that $In_{0.33}Tl_{0.67}P$ and $In_{0.85}Tl_{0.15}As$ are more robust than InSb, and much more so than $Hg_{1-x}Cd_xTe$, to the extent elastic constants are a meaningful indication of the resistance of a material to defects.[5] This offers strong evidence that these alloys are far less susceptible to the difficulties that plague $Hg_{1-x}Cd_xTe$, such as the high density of point and line defects deleterious to device performance and Hg loss on annealing, etc.

Table I shows that the lattice constants (a quantity predicted accurately by the LDA) of TlP, TlAs, and TlSb are 1.5–2% larger than those of InP, InAs, and InSb, respectively. Lattice matching is good, though slightly worse than in $Hg_{1-x}Cd_xTe$. $In_{0.33}Tl_{0.67}P$ matches to InP to within 1%, making InP an excellent substrate on which to grow $In_{1-x}Tl_xP$.

The LDA predicts negative gaps for TlP, TlAs, and TlSb; this continues to be the case after adjusting for errors in the

[a]Physics Department, Auburn University, Auburn, AL 36849.

 0003-6951/94/65(21)/2714/3/$6.00

TABLE I. Calculated (marked LD and GC) and experimental optical and structural properties for several ZB compounds at 0 K. For the Tl bearing compounds, data in the "Expt" column are taken from the calculations, adjusting for the LDA errors. a, lattice constant (Å); E_b, cohesive energy per atom (eV); $\hbar\omega_{TO}$, energy of the transverse optical mode Γ (meV); bulk modulus B and shear constant $c_{11}-c_{12}$ are in 10^{12} erg/cm^3. Energy gap marked +SO adds the spin-orbit splitting to the LDA gap. U and U/ϵ are the Coulomb repulsion, bare and screened. ITP, ITA, HCT: linear interpolation of the pure compounds to estimate properties of $In_{0.33}Tl_{0.67}P$, $In_{0.85}Tl_{0.15}As$, and $Hg_{0.78}Cd_{0.22}Te$.

	a		E_b			$\hbar\omega_{TO}$		B		$c_{11}-c_{12}$		Bandgap		Corrections			
	Expt	LD	Expt	LD	GC	Expt	LD	Expt	LD	Expt	LD	Expt	LD	+SO	U	U/ϵ	ΔE_g
InP	5.87	5.83	3.48	3.82	3.16	38.1	36.8	0.73	0.70	0.45	0.47	1.42	0.44	0.39	7.90	0.83	1.03
TlP	5.96	5.96	2.71	3.26	2.56		33.6		0.57		0.34	−0.27	−1.13	−1.18	7.86	0.46	0.86
InAs	6.06	6.04	3.10	3.59	2.88	27.3	26.3	0.58	0.59	0.38	0.39	0.42	−0.48	−0.62	7.69	0.65	1.04
TlAs	6.18	6.18	2.51	3.11	2.35		23.3		0.49		0.25	−1.34	−2.12	−2.26	7.65	0.38	0.78
InSb	6.48	6.46	2.80	3.30	2.59	22.6	21.7	0.48	0.45	0.31	0.32	0.26	−0.45	−0.72	6.99	0.45	0.98
TlSb	6.59	6.59	2.32	2.86	2.17		18.3		0.38		0.22	−1.60	−2.08	−2.35	6.95	0.35	0.75
CdTe	6.48	6.43	2.20	2.71	2.13	17.4	17.2	0.42	0.45	0.19	0.22	1.60	0.50	0.19	7.09	0.92	1.41
HgTe	6.46	6.45	1.62	2.20	1.53		13.7	0.42	0.46	0.19	0.20	−0.31	−0.93	−1.26	7.04	0.46	0.95
ITP	5.93	5.92	2.95	3.43	2.75		34.6		0.61		0.38						
ITA	6.08	6.06	3.01	3.52	2.80		25.9		0.58		0.37						
HCT	6.46	6.45	1.75	2.31	1.66		14.5	0.42	0.46	0.19	0.20						

LDA, as we now show. Because a reasonably rigorous theory to redress the error in the gap is difficult to implement, here we adopt a simpler theory of the bandgap underestimate due to Harrison.[6] Harrison notes that energy bands are calculated for a single potential; in the LDA, this potential stays fixed when an electron is excited to the conduction band. A more physically correct picture accounts for the electrostatic energy cost associated with the separation of electron and hole. This Harrison modeled by noting a coulombic repulsion U between the local excess charge and the excited electron. This repulsion is screened by surrounding medium so that the net energy cost, and correction to the bandgap is U/ϵ_∞. Harrison obtained U from a difference between the ionization potential and electron affinity of free atoms, taking an average of the cation and anion. Here we adopt the approach of Ref. 7, and calculate U in the local density approximation. Table I compares the experimental bandgap to the LDA gap, and also shows Harrison's theory for the bandgap correction. The latter systematically underestimates the correction by about 0.4 eV. Our predicted gap is obtained by adding Harrison's correction plus 0.4 eV to the LDA bandgap with the spin-orbit interaction included. We estimate the uncertainty in the gap to be about 0.1 eV.

By mapping the LDA bands onto a tight-binding hamiltonian, and correcting for errors mentioned above, we can examine the energy bands of TlP and TlAs. For the alloys, we employ the coherent potential approximation. This approach has been extensively tested in most ZB compounds and their alloys[8] and found to accurately model the composition dependence of the energy bands. Thus, apart from relatively small uncertainties in the TlP and TlAs band structures, the alloy hamiltonian should realistically model the experimental behavior. Near the gap, bands in TlP and HgTe are similar. We find $In_{1-x}Tl_xP$ and $In_{1-x}Tl_xAs$ possess a direct gap for all compositions x, with a significant bowing, particularly for $In_{1-x}Tl_xP$. Figure 1 shows that a gap of 0.1 eV is obtained at $1-x=0.33$ in $In_{1-x}Tl_xP$, and $1-x=0.85$ in $In_{1-x}Tl_xAs$; the lower inset of that figure displays the energy bands of $In_{0.33}Tl_{0.67}P$ and $Hg_{0.78}Cd_{0.22}Te$.

Electron mobilities in $Hg_{0.78}Cd_{0.22}Te$, $In_{0.33}Tl_{0.67}P$, and $In_{0.85}Tl_{0.15}As$ were calculated by a recently developed method to solve the Boltzmann equation with Fermi-Dirac statistics. This approach, which uses realistic energy bands and contains no adjustable parameters, predicts mobilities in $Hg_{0.78}Cd_{0.22}Te$ in very good agreement with experiment.[9] We find that mobilities of all three alloys are roughly 10^5 cm^2/V sec; the Tl-based alloys are usually somewhat larger owing to a smaller electron mass ($0.008m$ for $In_{0.33}Tl_{0.67}P$ and $0.0065m$ for $In_{0.85}Tl_{0.15}As$, compared with $0.009m$ in

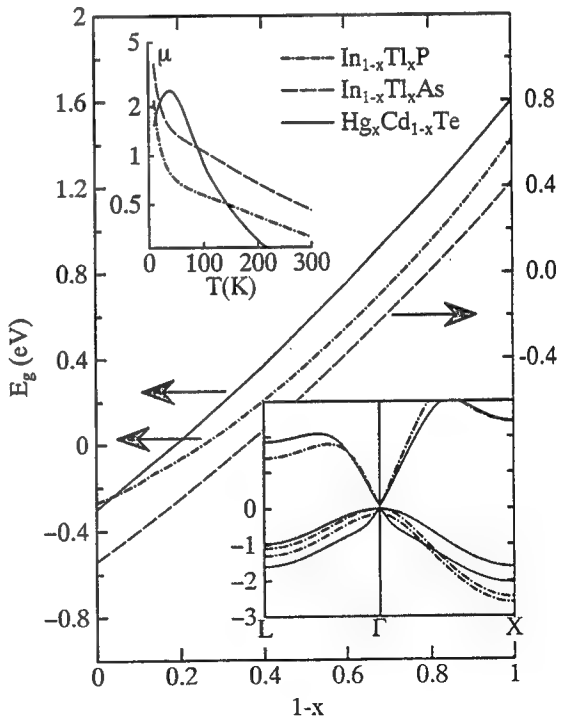

FIG. 1. Minimum bandgap in $Hg_{1-x}Cd_xTe$, $In_{1-x}Tl_xP$, and $In_{1-x}Tl_xAs$. (Note the energy scale is shifted by 0.8 eV for $In_{1-x}Tl_xAs$.) Upper inset: calculated electron mobility (in 10^5 cm^2/V sec) for $Hg_{0.78}Cd_{0.22}Te$, $In_{0.33}Tl_{0.67}P$, and $In_{0.85}Tl_{0.15}As$ vs temperature for a doping of 10^{14} cm^{-3}. Lower inset: energy bands of $In_{0.33}Tl_{0.67}P$, compared with those of $Hg_{0.78}Cd_{0.22}Te$. Bands of $In_{0.85}Tl_{0.15}As$ (not shown) appear similar to those of $In_{0.33}Tl_{0.67}P$.

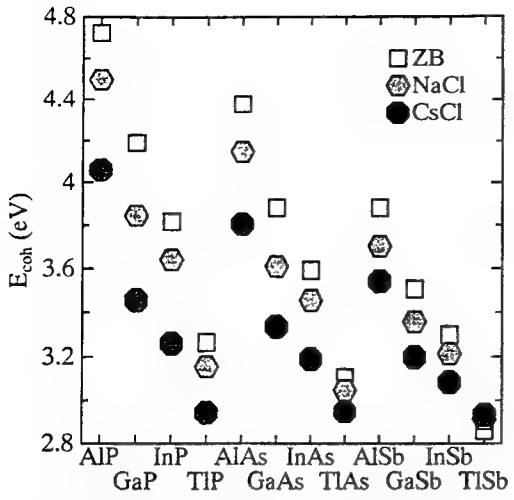

FIG. 2. Total energies of selected III-V compounds in the ZB, NaCl, and CsCl structures.

$Hg_{0.78}Cd_{0.22}Te$)/ However, in consequence their larger phonon energy (listed in Table I) and smaller density of states, the mobility in the Tl-based alloys can be smaller at low temperature. The upper inset of Fig. 1 compares the calculated mobility in the three alloys, for a doping of 10^{14} cm^{-3}. The calculated hole effective mass in the Tl-based alloys and $Hg_{1-x}Cd_xTe$ are approximately $0.37m$ and $0.65m$, respectively, suggesting a larger hole mobility in the Tl-based alloys.

We had suggested previously[1] that $In_{1-x}Tl_xSb$ might serve as an alternative to $Hg_{0.78}Cd_{0.22}Te$ in LWIR applications. We noted, however, that $In_{1-x}Tl_xSb$ suffers from one important drawback, namely that TlSb favors a more closely packed structure to the ZB. Subsequent attempts[2] to grow $In_{1-x}Tl_xSb$ have been hindered by the lack of a strong thermodynamic force driving Tl on the zinc-blende lattice. This difficulty apparently does not arise in either TlP or TlAs. Figure 2 epitomizes the question of structural stability of the Tl-bearing compounds, by comparing the binding energy of the ZB to the NaCl and CsCl structures for 12 III-V compounds. As expected, ZB is favored for the nine known compounds—those combining Al, Ga, and In with anions P, As, and Sb. We see that the ZB is favored particularly for the lighter, more strongly bound compounds. Next most favored is the six-fold coordinated NaCl structure; least favored is the close-packed CsCl structure. The preference for open structures reflects the ability of these compounds to form strong, directional bonds. As the binding becomes weak, the energy difference between the open and close-packed structures merge. In a bond-orbital picture, this can be understood as a weakening of the two-center bond. For the heavier elements, the "metallicity" [10] increases—the ratio of the energy gained by forming a bond to the energy cost needed to promote the atom to an sp^3 configuration. Indeed for TlSb, we see that both the NaCl and the CsCl structures overtake the ZB structure, as we had mentioned previously.[1] (One manifestation of this is the very negative bandgap in TlSb.) This reversal in the ordering of the energy complicates the growth of the $In_{1-x}Tl_xSb$ alloy, as we discussed in Ref. 1. Figure 2 shows that, in contrast, TlP and TlAs are stable relative to the more closely packed phases.

To summarize, we offer some persuasive evidence that $In_{1-x}Tl_xP$ and $In_{1-x}Tl_xAs$ form suitable materials for infrared detectors. $In_{1-x}Tl_xP$ in particular combines the best advantages of the current leading contenders: it is sturdy, with a direct gap tunable to the entire IR spectrum, and has a relatively modest lattice mismatch to InP. Thus, $In_{1-x}Tl_xP$/InP devices offer the potential support high-performance staring focal plane arrays (FPAs), with monolithic integration onto an ROIC chip.

Support from ONR Contracts N00014-88-C-0096 and N00014-89-K-0132 is gratefully acknowledged.

[1] M. van Schilfgaarde and A. Sher, Appl. Phys. Lett., **62**, 1857 (1993).
[2] Y. H. Choi, C. Besikci, R. Sudharsanan, and M. Razeghi, Appl. Phys. Lett. **64**, 462 (1994).
[3] M. van Schilfgaarde and M. Methfessel (unpublished). See M. Methfessel, Phys. Rev. B **38**, 1537 (1988) for a preliminary account.
[4] M. van Schilfgaarde and M. Berding, Bull. Am. Phys. Soc. **39**, 393 (1994).
[5] A. Sher, A.-B. Chen, W. E. Spicer, and K. C. Shi, J. Vac. Sci. Technol. A **3**, 105 (1985).
[6] W. A. Harrison, Phys. Rev. B **31**, 2121 (1985).
[7] M. van Schilfgaarde A. B. Chen, and A. Sher, Phys. Rev. Lett. **57**, 1149 (1986).
[8] A.-B. Chen and A. Sher, Phys. Rev. B **23**, 5360 (1981).
[9] S. Krishnamurthy and A. Sher, J. Appl. Phys. **75**, 7904 (1994).
[10] W. A. Harrison, *Electronic Structure and the Properties of Solids* (Freeman, San Franscisco, 1980).

Appendix B

InTIP—A PROPOSED INFRARED DETECTOR MATERIAL

InTlP — a Proposed Infrared Detector Material

M. van Schilfgaarde[a], An-Ban Chen[b], S. Krishnamurthy[a] and Arden Sher[a]

[a] *SRI International, Menlo Park, California 94025*

[b] *Physics Department, Auburn University, AL 36849*

(February 7, 1994)

Abstract

$In_{1-x}Tl_xP$ is proposed as a promising material for infrared detectors. A number of key optical and structural properties are studied within local density-functional theory. $In_{1-x}Tl_xP$ at x=0.33 and $In_{1-x}Tl_xAs$ at x=0.85 are estimated to have a gap of 0.1 eV. Their binding energies are larger than that of InSb, and they are found to form stable zincblende alloys for all x. $In_{1-x}Tl_xP$ nearly lattice matches to InP, and offers the potential to integrate detector array and read-out circuit.

PACS 61.50Cj 61.55Hg 81.30Dz 78.30Fs 64.70Kb 64.70Dv

than InAs, and $In_{1-x}Tl_xP$ offers the advantage of monolithic integration onto an ROIC chip.

Let us assume for the moment that TlP and TlAs can be grown in a zincblende structure, and compare some of their key structural properties to those of CdTe and HgTe, as predicted by local density-functional theory. Table I lists some such properties, which were calculated by a full-potential version of the LMTO method.[3] All-electron density functional calculations predict mechanical and structural properties in good agreement with experiment for all known ZB semiconductors,[4], as Table I shows for the compounds listed. Errors in the LDA are small but systematic;[4] because we wish to use the LDA to predict properties of compounds as yet unmade, we make corrections to the LDA to arrive at the predicted values in Table I.

For the cohesive energy we can estimate the LDA errors by including gradient corrections to the local density-functional. The gradient corrections are found to eliminate, and indeed slightly overcorrect for the LDA overbinding in the zincblende compounds[4], as we see in Table I for the known compounds listed. Binding in TlP is comparable to InSb, and far stronger than in HgTe. Also listed are data linearly interpolated for the alloys $In_{0.33}Tl_{0.67}P$, $In_{0.85}Tl_{0.15}As$ and $Hg_{0.78}Cd_{0.22}Te$ (compositions which are predicted to produce a 0.1 eV bandgap, as we discuss later). The relatively large elastic constants are another indication that TlP and TlAs are relatively robust ZB compounds, with a chemical bond and mechanical properties comparable to those of InAs. They suggest that $In_{0.33}Tl_{0.67}P$ and $In_{0.85}Tl_{0.15}As$ are more robust than InSb, and much more so than $Hg_{1-x}Cd_xTe$, to the extent elastic constants are a meaningful indication of the resistance of a material to defects.[5] This offers strong evidence that these alloys are far less susceptible to the difficulties that plague $Hg_{1-x}Cd_xTe$, such as the high density of point and line defects deleterious to device performance and Hg loss on annealing, *etc.*

Table I shows that the lattice constants (a quantity predicted accurately by the LDA) of TlP, TlAs and TlSb are 1.5–2% larger than those of InP, InAs and InSb, respectively. Lattice matching is good, though slightly worse than in $Hg_{1-x}Cd_xTe$. $In_{0.33}Tl_{0.67}P$ matches to InP to within 1%, making InP an excellent substrate on which to grow $In_{1-x}Tl_xP$.

Electron mobilities in $Hg_{0.78}Cd_{0.22}Te$, $In_{0.33}Tl_{0.67}P$ and $In_{0.85}Tl_{0.15}As$ were calculated by recently developed method to solve the Boltzmann equation with Fermi-Dirac statistics. This approach, which uses realistic energy bands and contains no adjustable parameters, predicts mobilities in $Hg_{0.78}Cd_{0.22}Te$ in very good agreement with experiment.[9] We find that mobilities of all three alloys are roughly $10^5 cm^2/V\text{-}sec$, the Tl-based alloys usually somewhat larger owing to a smaller electron mass ($0.008m$ for $In_{0.33}Tl_{0.67}P$ and $0.0065m$ for $In_{0.85}Tl_{0.15}As$, compared with $0.009m$ in $Hg_{0.78}Cd_{0.22}Te$.) However, in consequence their larger phonon energy (listed in Table I) and smaller density of states, the mobility in the Tl-based alloys can be smaller at low temperature. The upper inset of Fig. 1 compares the calculated mobility in the three alloys, for a doping of $10^{14}cm^{-3}$. The calculated hole effective mass in the Tl-based alloys and $Hg_{1-x}Cd_xTe$ are approximately $0.37m$ and $0.65m$, respectively, suggesting a larger hole mobility in the Tl-based alloys.

We had suggested previously[1] that $In_{1-x}Tl_xSb$ might serve as an alternative to $Hg_{0.78}Cd_{0.22}Te$ in LWIR applications. We noted, however, that $In_{1-x}Tl_xSb$ suffers from one important drawback, namely that TlSb favors a more closely packed structure to the ZB. Subsequent attempts[2] to grow $In_{1-x}Tl_xSb$ have been hindered by the lack of a strong thermodynamic force driving Tl on the zincblende lattice. This difficulty apparently does not arise in either TlP or TlAs. Fig. 2 epitomizes the question of structural stability of the Tl-bearing compounds, by comparing the binding energy of the ZB to the NaCl and CsCl structures for 12 III-V compounds. As expected, ZB is favored for the nine known compounds—those combining Al, Ga and In with anions P, As and Sb. We see that the ZB is favored particularly for the lighter, more strongly bound compounds. Next most favored is the 6-fold coordinated NaCl structure; least favored is the close-packed CsCl structure. The preference for open structures reflects the ability of these compounds to form strong, directional bonds. As the binding becomes weak, the energy difference between the open and close-packed structures merge. In a bond-orbital picture, this can be understood as a weakening of the two-center bond. For the heavier elements, the "metallicity"[10] increases—the ratio of the energy gained by forming a bond to the energy cost needed to promote the

REFERENCES

[1] M. van Schilfgaarde and A. Sher, *Appl. Phys. Lett.*, **62**, 1857 (1993).

[2] Y. H. Choi, C. Besikci, R. Sudharsanan and M. Razeghi, *Appl. Phys. Lett.*, **64**, 462 (1994).

[3] M. Methfessel and M. van Schilfgaarde, in preparation.

[4] M. van Schilfgaarde, M. Berding and M. Methfessel in preparation.

[5] A. Sher, A.-B. Chen, W. E. Spicer and K. C. Shi, J. Vac. Sci. Technol. **A3**, 105 (1985).

[6] W. A. Harrison, Phys. Rev. **B31**, 2121 (1985).

[7] M. van Schilfgaarde A. B. Chen and A. Sher, *Phys. Rev. Lett.* **57**, 1149 (1986).

[8] A.-B. Chen and A. Sher, *Semiconductor Alloys,* (Plenum, 1994) [unpublished].

[9] S. Krishnamurthy and A. Sher, submitted to *J. Appl. Phys.*

[10] W. A. Harrison, *Electronic Structure and the Properties of Solids*, Freeman (1980).

TABLES

TABLE I. Calculated (marked *LD* and *GC*) and experimental optical and structural properties for several ZB compounds at 0°K. For the Tl bearing compounds, data in the "Expt" column are taken from the calculations, adjusting for the LDA errors. a, lattice constant (Å); E_b: cohesive energy per atom (eV); $\bar{h}\omega_{TO}$, energy of the transverse optical mode Γ (meV); bulk modulus B and shear constant c_{11}-c_{12} are in (10^{12}erg/cm^3). Energy gap marked $+SO$ adds the of spin-orbit splitting to the LDA gap. U and U/ϵ are the coulomb repulsion, bare and screened. ITP, ITA, HCT: linear interpolation of the pure compounds to estimate properties of $In_{0.33}Tl_{0.67}P$, $In_{0.85}Tl_{0.15}As$ and $Hg_{0.78}Cd_{0.22}Te$.

	a		E_b			$\hbar\omega_{TO}$		B		$c_{11}-c_{12}$		Bandgap			Corrections		
	Expt	*LD*	*Expt*	*LD*	*GC*	*Expt*	*LD*	*Expt*	*LD*	*Expt*	*LD*	*Expt*	*LD*	$+SO$	U	U/ϵ	ΔE_g
InP	5.87	5.83	3.48	3.82	3.16	38.1	36.8	0.73	0.70	0.45	0.47	1.42	0.44	0.39	7.90	0.83	1.03
TlP	5.96	5.96	2.71	3.26	2.56		33.6		0.57		0.34	-0.27	-1.13	-1.18	7.86	0.46	0.86
InAs	6.06	6.04	3.10	3.59	2.88	27.3	26.3	0.58	0.59	0.38	0.39	0.42	-0.48	-0.62	7.69	0.65	1.04
TlAs	6.18	6.18	2.51	3.11	2.35		23.3		0.49		0.25	-1.34	-2.12	-2.26	7.65	0.38	0.78
InSb	6.48	6.46	2.80	3.30	2.59	22.6	21.7	0.48	0.45	0.31	0.32	0.26	-0.45	-0.72	6.99	0.45	0.98
TlSb	6.59	6.59	2.32	2.86	2.17		18.3		0.38		0.22	-1.60	-2.08	-2.35	6.95	0.35	0.75
CdTe	6.48	6.43	2.20	2.71	2.13	17.4	17.2	0.42	0.45	0.19	0.22	1.60	0.50	0.19	7.09	0.92	1.41
HgTe	6.46	6.45	1.62	2.20	1.53		13.7	0.42	0.46	0.19	0.20	-0.31	-0.93	-1.26	7.04	0.46	0.95
ITP	5.93	5.92	2.95	3.43	2.75		34.6		0.61		0.38						
ITA	6.08	6.06	3.01	3.52	2.80		25.9		0.58		0.37						
HCT	6.46	6.45	1.75	2.31	1.66		14.5	0.42	0.46	0.19	0.20						

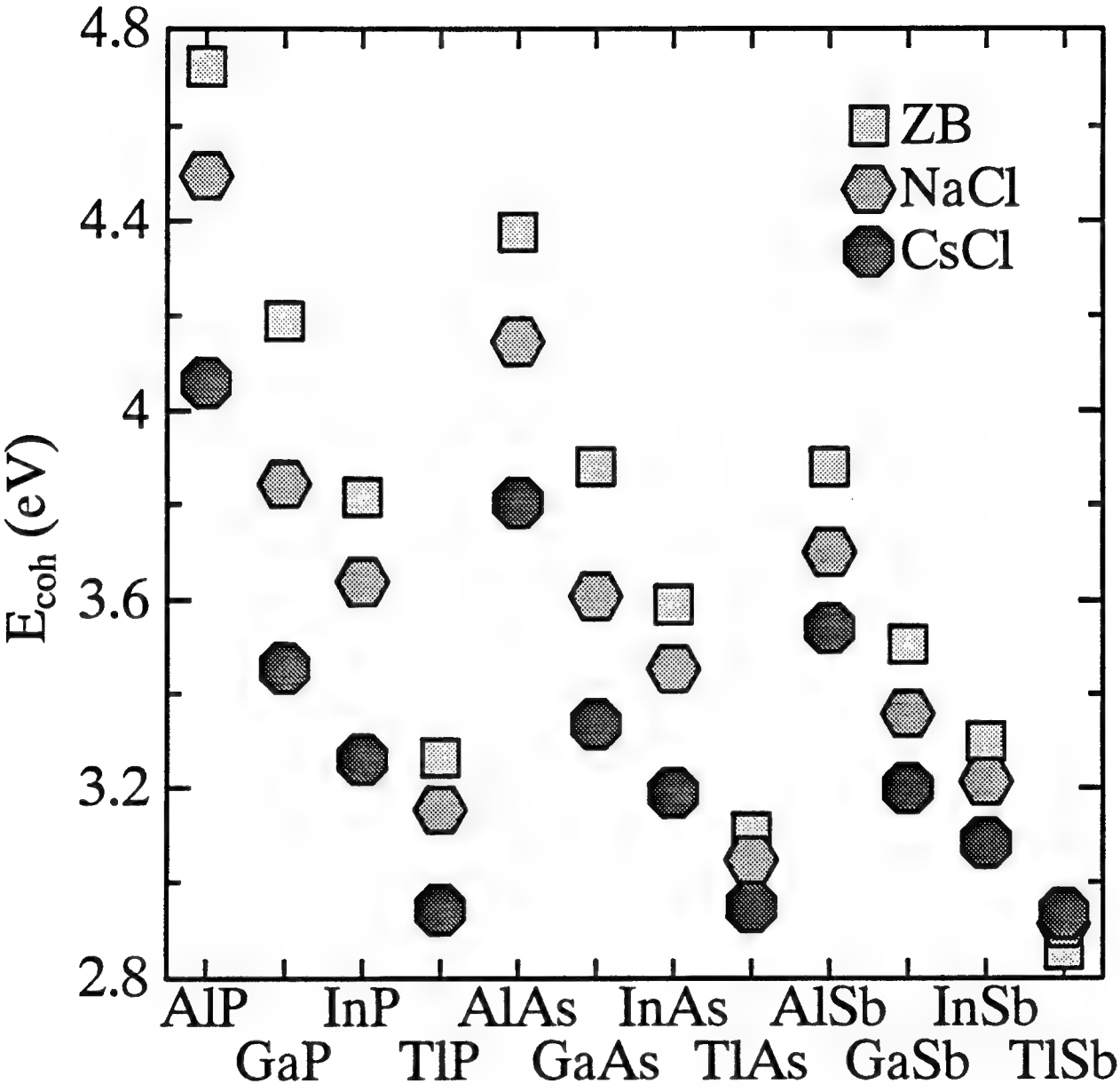
4.8
4.4
4
3.6
3.2
2.8
E_{coh} (eV)
ZB
NaCl
CsCl
AlP
InP
AlAs
InAs
AlSb
InSb
GaP
TlP
GaAs
TlAs
GaSb
TlSb

Fig 2

Appendix C

TEMPERATURE DEPENDENCE OF BAND GAPS IN HgCdTe AND OTHER SEMICONDUCTORS

Temperature Dependence of Band Gaps in Hgcdte and Other Semiconductors

Srinivasan Krishnamurthy[a], A.-B. Chen[b], A. Sher[a], and M. van Schilfgaarde[a]

[a] *SRI International, Menlo Park, CA 94025*

[b] *Physics Department, Auburn University, Auburn, AL 36849*

(September 27, 1994)

Abstract

Band-edge shifts induced by the electron-phonon interaction are calculated for HgCdTe alloys and various semiconductor compounds starting from accurate zero-temperature band structures. The calculated temperature variation of gaps agrees with experiments to better than 10% in all materials except InAs and InSb where the deviation is about 50%. While the simple picture that the intra (inter)-band transitions reduce (increase) the gap still holds, we show that both the conduction band edge E_c and valence band edge E_v move down in energy. These shifts in E_v affect the valence band offsets in heterojunctions at finite temperature. The temperature variations of valence band offset and the electron effective mass are also reported.

Key words: Temperature-dependent band structures, electron-phonon interactions, band offset, HgCdTe and alloys, III-V semiconductors

INTRODUCTION

The temperature (T) dependence of energy gaps of semiconductors is of great physical and technological interest. The quantities such as band offset and effective mass depend sensitively on the temperature variation of band edges. Numerous theoretical [1-9] and experimental [10-19] studies have been undertaken to obtain both qualitative and quantitative variations of various gaps in semiconductors. The gap decreases with increasing temperature in medium-gap and wide-gap semiconductors, and it increases in small-gap materials such as HgCdTe, PbS, PbSe, and PbTe. The thermal expansion of the lattice and electron-phonon interactions are usually considered causes for the temperature variation of the band structures. Thermal expansion always reduces gaps.

In a perturbation-theory treatment of electron-phonon interactions, the intraband transitions reduce the gap whereas interband transitions increase it, and the net shift in the gap can be positive or negative. Here we calculate the gap variation in $Hg_{1-x}Cd_xTe$ alloys, GaAs, InAs, InSb, InP, and CdTe compounds, starting from accurate band structures, wave functions, proper phonon dispersion relations, and taking account of matrix elements of the electron-phonon interactions. The contributions from each phonon branch to each electron band have been obtained to assist physical understanding of the underlying causes of the variations. We show that *both* conduction and valence band edges move down in energy. When the valence band edge moves more than the conduction band edge, the gap increases with T, as in the case of some $Hg_{1-x}Cd_xTe$ alloys with $x < 0.5$. The reverse occurs for all III-V compounds studied and $Hg_{1-x}Cd_xTe$ with $x > 0.5$. This observation has an important effect on our understanding of the variation of band offsets in semiconductor heterojunctions. In addition to the gap, other features of the band structure change with temperature and will affect the spectral variations of the absorption coefficient and transport properties.

METHOD

Our calculation of the temperature dependence of the band gap starts with accurate band structures. Empirical pseudopotential form factors are used to construct a hybrid pseudopotential tight-binding (HPTB) Hamiltonian. The pseudopotential part of the Hamiltonian is universal– it applies to all group IV, III-V and II-VI compounds. The smaller tight-binding part is expressed in a minimum set of sp^3 Slater orbitals per atom. This Hamiltonian is then transformed into an orthonormal basis. A site-diagonal spin-orbit Hamiltonian is then added. Parameters in the tight-binding perturbation are chosen to fine-tune the band structures to agree well with experiments [20,21]. Various results obtained using these band structures are found to be quite reliable [21-23]. The present study subjects the accuracy of the wave functions as well as the energies to a sensitive test.

The dilation contribution to the band gap reduction is given [5,9] by $3\alpha_T \mathrm{B}\partial E_g/\partial \mathrm{P}$, where the thermal expansion coefficient of the lattice α_T, the bulk modulus B, and the change in the gap with pressure are obtained from the literature [19]. The electron-phonon interactions with all phonon branches that cause the band structure changes are treated in perturbation theory. The total Hamiltonian is assumed to be a sum of potentials from single atoms. The atomic potential in the solid is traditionally expanded in a Taylor series, with only the leading term retained, and the energy shifts it causes are evaluated in second-order perturbation theory. However, it has been demonstrated by a number of researchers [3,4,6] that retention of first-order perturbation terms with a second term in the Taylor series expansion is necessary to preserve symmetry. We retain both terms. The change in the energy at a given wave vector k is

$$\Delta E_{n\mathbf{k}} = < n\mathbf{k}|V_2|n\mathbf{k} > + \sum_{n'\mathbf{k}'} \frac{| < n'\mathbf{k}'|V_1|n\mathbf{k} > |^2}{E_{n\mathbf{k}} - E_{n'\mathbf{k}'}} \qquad (1)$$

where V_1 and V_2 are the first two terms in the Taylor expansion of the total electron-phonon potential in powers of atomic displacements ξ. In the TB formalism, Eq. (1) can be written in terms of the matrix elements

$$< l'j'\alpha'|V_1|lj\alpha >= \nabla V_{\alpha\alpha'}(\mathbf{d}_{ll'}^{jj'}) \cdot (\xi_{l'j'} - \xi_{lj}), \tag{2}$$

and

$$< l'j'\alpha'|V_2|lj\alpha > = \tfrac{1}{2}[\xi_{l'j'} \cdot (\nabla)^2 V_{\alpha\alpha'}(\mathbf{d}_{ll'}^{jj'}) \cdot \xi_{l'j'} + \xi_{lj} \cdot (\nabla)^2 V_{\alpha\alpha'}(\mathbf{d}_{ll'}^{jj'}) \cdot \xi_{lj}], \tag{3}$$

where $\mathbf{d}_{ll'}^{jj'}$ is the position vector connecting atomic sites l, species (anion or cation) j and site l', species j', and $V_{\alpha\alpha'}$ $(\mathbf{d}_{ll'}^{jj'})$ is a HPTB matrix element between the orbitals α and α' located on those atoms. From the quantum theory of harmonic crystals, the atomic displacements ξ can be expressed in terms of normal modes– that is, phonons. We have

$$\xi_{lj} = [\tfrac{\hbar}{2NM_j}]^{\frac{1}{2}} \sum_{\mathbf{q}\lambda} \omega_{\lambda\mathbf{q}}^{-\frac{1}{2}} [\mathbf{e}_{\lambda\mathbf{q}}^{j} a_{\lambda\mathbf{q}} e^{i\mathbf{q}\cdot(l+\tau_j)} + \mathbf{e}_{\lambda\mathbf{q}}^{*j} a_{\lambda\mathbf{q}}^{\dagger} e^{-i\mathbf{q}\cdot(l+\tau_j)}] \tag{4}$$

where $\mathbf{q}$ and ω are phonon wave vector and frequency, λ denotes phonon branch, a($a^{\dagger}$) is a phonon annihilation (creation) operator, M is the atomic mass, and $\mathbf{e}$ is an eigenvector in a diamond or zincblende structure of the six-dimensional dynamical matrix eigenvalue problem

$$M\omega^2\mathbf{e} = \mathbf{D}(\mathbf{q})\mathbf{e} \tag{5}$$

Evaluation of the matrix elements given by Eqs. (2) and (3) requires knowledge of spatial variations of the interatomic TB matrix elements $V_{\alpha\alpha'}$. In Harrison's universal TB approach [24], these matrix elements scale as d^{-2}. In our generalization, we assume that $V_{\alpha\alpha'}$ varies as d^{-m} and the repulsive first-neighbor pair energy, following Harrison's overlap argument, as η/d^{2m}. The two unknowns m and η are determined by requiring that the calculated equilibrium bond length and bulk modulus agree well with experiments. This approach, with electrons and phonons treated from the same underlying Hamiltonian, has previously been used successfully to explain hot electron transistor characteristics [23] and is also in fairly good agreement with first-principles calculations [25]. The dynamical matrix $\mathbf{D}$ is calculated from the valence force field model [26].

The calculational procedure is as follows. For a chosen material, m and η are evaluated. Then the first and second derivatives of all interatomic matrix elements are obtained. The dynamical matrix is diagonalized to obtain ω and **e** as a function of **q** and λ. The phonon structures and electronic band structures are used [Eqs. (1) through (4)] to obtain the change in the band energy at a given **k**. The polar coupling terms are included in the longitudinal optical phonon contributions. When we are interested in studying the change in the direct gap, **k** is taken to be zero. However, when the temperature variation of the effective masses or indirect gap are studied, non-zero **k** values must be used and the Brillouin zone summation in Eq. (1) should be carried over the entire zone with reduced, or no, symmetry.

RESULTS

The calculated band-gap change as a function of T in $Hg_{0.78}Cd_{0.22}Te$ is shown in Fig. 1. With increasing T, the direct gap increases in $Hg_{0.78}Cd_{0.22}Te$. Notice that the calculated values are typically within 10 to 15 meV of experimental values [16-18]. The cross ($\times$) at T=0 represents the calculated zero-point correction to the gap (13.6 meV for $Hg_{0.78}Cd_{0.22}Te$). The zero-temperature band gap calculated without electron-phonon interactions should have this correction subtracted for comparison to experimental values.

The change in the gap is traditionally explained in terms of inter- and intraband interactions. The intravalence (conduction) band interactions push the valence (conduction) band edge up (down), thus reducing the gap. Similarly, the valence-conduction band interactions increase the gap. Hence, one might expect the gap to decrease in wide-gap semiconductors and possibly increase in small-gap semiconductors. In addition, arguments based only on total density of states and ignoring variations in matrix elements will predict the valence band edge E_v move up in energy, because the hole effective mass is one to two orders of magnitude larger than the electron mass. As seen from Fig. 2, our detailed calculations of band edge movements in $Hg_{0.78}Cd_{0.22}Te$ do not support this traditional view. We find that

both E_c and E_v (solid lines) move down in energy. This same trend is observed in other semiconductor compounds studied (GaAs, InP, InAs, InSb, and GaSb). The movement of the valence (solid line) and conduction (dashed) band edges due to interaction with other bands is also shown in Fig. 2. The interaction of the band edges with the conduction bands (CBs) is much stronger than with valence bands (VBs), and consequently both E_v and E_c move down in energy. E_v moves much more than E_c and the gap increases.

We analyze the strength of inter- and intraband electron-phonon interactions by presenting the contributions from each band and from each phonon mode. Table 1 lists the calculated values for $Hg_{0.78}Cd_{0.22}Te$ at 300 K. Although spin is included in our band structure calculations, only spin averaged values are listed. Band indices 1 to 4 correspond to VBs, and the others to CBs. The first two rows show changes in E_v and E_c due to interactions with various bands. Contributions from each phonon mode are listed in the remaining rows. The lowest VB is about 12 eV below E_v and E_c, and hence the interaction does not affect the band edges. We see that the interaction with other VBs tend to push the band edges up in energy, as expected. Note that the top two valence bands contribute the most to the fundamental band-edge changes. However, interaction of the band edges with CBs is even stronger and negative. Particularly, the interaction of E_v with all conduction bands is strong. As E_v moves down more than E_v, the gap increases in $Hg_{0.78}Cd_{0.22}Te$. To understand the role of various phonons, we display the contribution from each mode separately. The phonon-induced changes in the band edges at 300 K in $Hg_{0.78}Cd_{0.22}Te$ are listed in the third through tenth rows of Table 1. We see that acoustic phonons account for about 75% of the total change in the valence and conduction band-edge energies. The selection rules wipe out interband matrix elements in spite of the stronger coupling constant between electrons and polar longitudinal phonons, so they do not dominate this phenomenon as they do with mobilities, which depend on intraband matrix elements.

Our calculations for other compounds show a qualitatively similar role for phonons. In addition to $Hg_{0.78}Cd_{0.22}Te$, we studied the band-gap variation with temperature in GaAs, InAs, InP, InSb, GaSb, and CdTe compounds and HgCdTe alloys. The gap changes linearly

at high temperatures (>150 K). The calculated dE_g/dT values (circle) are compared with experiments (cross) values in Fig. 3. We see that the calculations produced correct trends in all these materials, but compare less favorably with experiments in InAs and InSb. However, it is important to note that the sign of the change is not exclusively determined by the magnitude of the zero-temperature gap. For example, although $Hg_{0.70}Cd_{0.30}Te$ and InSb have the same zero-temperature gap of 0.235 eV, the InSb gap decreases with T, whereas the $Hg_{0.70}Cd_{0.30}Te$ gap increases with T. The combination of gap size, conduction band width, and intervalley separations gives rise to these interesting variations in the gap with T.

The observation that both E_v and E_c move down in energy has an important effect on band offsets in heterojunction-based devices. For example, the zero-temperature valence band offset between $Hg_{0.78}Cd_{0.22}Te$ and CdTe is believed to be around 350 meV. However, we find that at 300 K, E_v in $Hg_{0.78}Cd_{0.22}Te$ and in CdTe moves down by 215 meV and 30 meV, respectively. If the dipole contribution remains the same, the valence band offset decreases to 165 meV at 300 K. The contention that the dipole contribution is nearly temperature independent stems from the observation that any shift in the average effective crystal potentialshould effectively be screened out, since these semiconductors are good dielectrics ($\epsilon \geq 10$). The temperature variation of the bands should be taken with respect to a fixed average potential. For our Hamiltonian, the valence band edge movements in each side of the junction are calculated with reference to a fixed average state. Thus, the calculated temperature dependence of the difference in the VB edge of the constituent heterojunction materials effectively governs the temperature dependence of the band offset. In addition to the electron-phonon interactions discussed above, lattice dilation changes the band edges differently [9]. This effect is not included here. In any case, this band offset change has important implications for the design of abrupt heterojunction IR absorption and confined well laser devices.

In principle, the band structure at any wave vector k will change with temperature. With the change in the fundamental gap, the band curvature (or effective mass) also changes thus

affecting the optical and transport properties of the material. The self-energy calculated in this method will include the effect of scattering due to phonons *and* the change in the temperature-dependent band structure self-consistently. In the case a of narrow-gap material such as $Hg_{0.78}Cd_{0.22}Te$, the effective mass alone does not explain the low-energy portion of the conduction band structure. The lowest CB energy at any k is best described by a hyperbola [27], $(\gamma \mathbf{k}^2 + c^2)^{1/2} - c$. The calculated band gap, effective mass, γ, and c as functions of T are given in Table 2. The effective mass and c are directly proportional to the gap and hence monotonically increase with T. This is expected from the $\mathbf{k} \cdot \mathbf{P}$ theory argument, but the magnitudes predicted by two theories differ. γ decreases slightly at lower temperatures and then starts to increase with T. In a previous publication [27], we had simulated these temperature variations of γ and c by adjusting the Hg concentration in HgCdTe alloys to produce proper gap at each temperature. Those values are in remarkable agreement with the values reported in Table 2. We conclude that γ and c (given in Table 2) can be interpolated to considerable accuracy for any positive gap in the HgCdTe alloys

CONCLUSIONS

Although the calculations produced correct trends in all materials, the calculated changes in the band gap of InAs and InSb were about a factor of 2 smaller than in the experiments. We find that our calculated TA phonon frequencies away from zone center in these compounds were considerably larger than those found in experiments. As noted from Table 1, a substantial contribution comes from acoustic phonons. Consequently, our theoretical values of $E_g(T)$ are smaller than in experiments. Better predictability should result from improvement in the dynamical matrix calculated from the underlying Hamiltonian. In addition, at higher temperatures higher-order perturbation terms must be included along with finite-temperature 'renormalized' bands rather than the zero-temperature bands. Such renormalization affects the monotonic change in the gap and introduces nonlinear terms.

In summary, we have calculated the temperature variations of band gaps in various semi-

conductors. A fairly accurate HPTB Hamiltonian is used in the calculation of electron and phonon structures. The calculations explain the increase in the band gap of $Hg_{0.78}Cd_{0.22}Te$, and the decrease in the band gap of all III-V compounds studied. We show that acoustic phonons make the major contribution. Contrary to traditional thinking based on total density of states arguments, we find that both the valence and the conduction band edges move down in energy. One important consequence of this observation will be in the band offsets in semiconductor heterojunction devices. Finally, there is a small and usually negligible zero-point motion contribution to low-temperature band gaps arising from electron-phonon interactions.

We thank Dr. M. Cardona of the Max Planck Institute, Stuttgart, for pointing us to several references. Funding from ONR (contract N00014-93-C-0091) and ARPA (contract MDA972-92-C-0053) is gratefully acknowledged.

REFERENCES

[1] Y. P. Varshini, Physica **34**, 149 (1967).

[2] V. Heine and J .A. Van Vechten, Phys. Rev. B**13**, 1622 (1976).

[3] P. B. Allen and V. Heine, J. Phys. C **9**, 2305 (1976).

[4] P. B. Allen and M. Cardona, Phys. Rev. B **27**, 4760 (1983).

[5] S. Gopalan, P. Lautenschlager, and M. Cardona, Phys. Rev. B **35**, 5577 (1987).

[6] M. Cardona and S. Gopalan, in *Progress on electron properties of solids*, R. Girlanda *et al.*, eds. (Kluwer Academic publishers, 1989), p. 52.

[7] R. D. King-Smith, R. J. Needs, V. Heine, and M. J. Hodgson, Europhys. Lett. **10**, 569 (1989).

[8] S. Zollner, S. Gopalan, and M. Cardona, Sol. State Comm. **77**, 485 (1991).

[9] K. J. Malloy and J. A. Van Vechten, J. Vac. Sci. Technol. B **9**, 2112 (1991).

[10] P. Lautenschlager, M. Garriga, S. Logothetidis, and M. Cardona, Phys. Rev. B **35**, 9174 (1987), and references cited therein.

[11] Z. Hang, D. Yan, F. H. Pollak, G. D. Pettit, and M. Woodall, Phys. Rev. B **44**, 10546 (1991).

[12] L. Pavisi, F. Piazza, A. Rudra, J. F. Carlin, and M. Ilegems, Phys. Rev. B **44**, 9052 (1991).

[13] E. Grilli, M. Guzzi, R. Zamboni, and L. Pavesi, Phys. Rev. B **45**, 1638 (1992).

[14] P. Y. Liu and J. C. Maan, Phys. Rev. B **47**, 16274 (1993).

[15] M. E. Allali, C. B. Sorenson, E. Veje, and P. T. Petersson, Phys. Rev. B **48**, 4398 (1993).

[16] G. L. Hansen, J. L. Schmit, and T. N. Casselman, J. Appl. Phys. **53**, 7099 (1982).

[17] D. G. Seiler, J. R.Lowney, C. L. Littler, and M. R. Loloee, J. Vac. Sci. Technol. **A 8**, 1237 (1990).

[18] J. C. Brice, *Properties of mercury cadmium telluride*, J. Brice and P. Capper, eds. (EMIS datareviews series 3, INSPEC publication, 1987), p. 105.

[19] *Landolt-Börnstein Numerical data and functional relationships in science and technology*, Madelung, Schultz and Weiss (eds.), New series, Vol. 17 (1982).

[20] A. -B. Chen and A. Sher, Phys. Rev. B **23**, 5360 (1981).

[21] S. Krishnamurthy, A. -B. Chen, and A. Sher, J. Appl. Phys. **63**, 4540 (1988).

[22] S. Krishnamurthy, A. Sher, and A. -B. Chen, Phys. Rev. Lett., **64**, 2531 (1990); Appl. Phys. Lett **55**, 1002 (1989); Appl. Phys. Lett **52**, 468 (1988).

[23] S. Krishnamurthy, A. Sher, and A. -B. Chen, Appl. Phys. Lett. **53**, 1853 (1988).

[24] W. Harrison, *Electronic structure and properties of solids* (Freeman, San Francisco, 1980).

[25] S. Krishnamurthy and M. Cardona, J. Appl. Phys. **74**, 2117 (1993).

[26] R. M. Martin, Phys. Rev. **B1**, 4005 (1970).

[27] S. Krishnamurthy, and A. Sher, J. Elec. Materials. (in Press) Presented at the 1993 MCT workshop, Seattle.

TABLES

TABLE 1. Calculated change in the valence (v) and conduction (c) band edge energies (in meV) of $Hg_{0.78}Cd_{0.22}Te$ alloy. Contributions from interaction with various phonon modes are shown in rows 3 to 10.

band		1	2	3	4	5	6	7	8
	v	5.90	13.99	56.85	88.51	-80.26	-92.49	-97.45	-102.07
Total									
	c	1.04	2.84	17.27	34.07	-23.81	-25.43	-43.96	-42.48
	v	4.03	6.21	30.06	41.52	-49.86	-62.17	-61.04	-49.62
TA									
	c	0.26	0.65	12.41	27.47	-3.58	-14.81	-24.50	-15.40
	v	0.91	3.18	3.14	10.53	-10.63	-5.92	-11.41	-20.59
LA									
	c	0.56	1.29	1.27	1.72	-14.94	-3.00	-2.66	-7.17
	v	0.33	2.11	6.12	11.22	-9.52	-4.98	-11.80	-17.40
LO									
	c	0.13	0.63	0.75	0.44	-3.78	-2.45	-1.18	-7.31
	v	0.63	2.48	17.53	25.24	-10.26	-19.42	-13.20	-14.45
TO									
	c	0.10	0.27	2.84	4.44	-1.52	-5.16	-15.62	-12.59

TABLE 2. Calculated E_g [meV], γ [eV^2], c[eV] and the effective mass ratio of $Hg_{0.78}Cd_{0.22}Te$ alloy as functions of temperature. $m^*(0)$ is 0.008. The zero point correction is 13.6 meV.

T	E_g	γ	c	$m^*(T)/m^*(0)$
1.00	113.60	47.7656	0.0588	1.0000
10.00	112.67	47.7553	0.0588	1.0005
20.00	112.56	47.7169	0.0592	1.0072
30.00	114.44	47.6421	0.0598	1.0199
40.00	117.15	47.5582	0.0607	1.0361
50.00	120.42	47.4461	0.0615	1.0532
60.00	123.96	47.3310	0.0624	1.0714
70.00	127.65	47.2091	0.0634	1.0904
80.00	131.44	47.0821	0.0643	1.1095
90.00	135.28	46.9418	0.0653	1.1288
100.00	139.17	46.7964	0.0662	1.1483
150.00	158.85	46.1544	0.0712	1.2529
200.00	178.73	45.5930	0.0767	1.3669
250.00	198.68	45.2441	0.0832	1.4938
300.00	218.66	45.1167	0.0908	1.6342
350.00	238.65	45.3460	0.1000	1.7913
400.00	258.66	46.0193	0.1115	1.9672
450.00	278.67	47.3751	0.1263	2.1657
500.00	298.69	49.8338	0.1468	2.3919
550.00	318.71	54.0581	0.1763	2.6491
600.00	338.74	61.7125	0.2238	2.9445

FIGURES

FIG. 1. Change in the band gap of $Hg_{0.78}Cd_{0.22}Te$ with temperature.

FIG. 2. Variation of conduction (dashed line) and valence (solid line) band edges of $Hg_{0.78}Cd_{0.22}Te$ with temperature.

FIG. 3. Derivative of direct gap with temperature for various semiconductor compounds and alloys as a function of zero-temperature gap. The vertical lines represent $Hg_{0.78}Cd_{0.22}Te$, InSb, InAs, $Hg_{0.5}Cd_{0.5}Te$, InP, GaAs and CdTe, respectively.

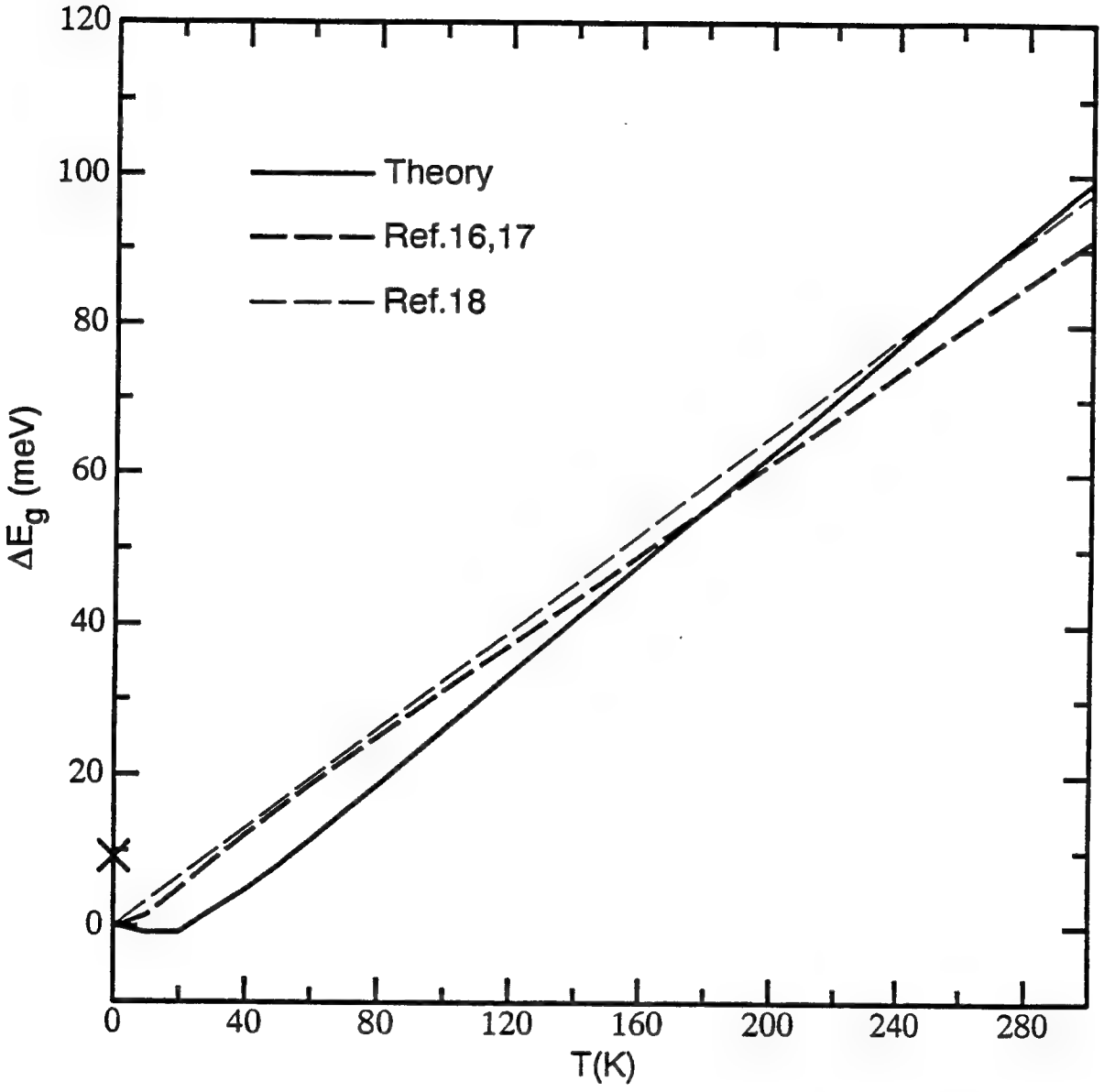
120
100
80
60
40
20
0
ΔE_g (meV)
Theory
Ref.16,17
Ref.18
0
40
80
120
160
200
240
280
T(K)

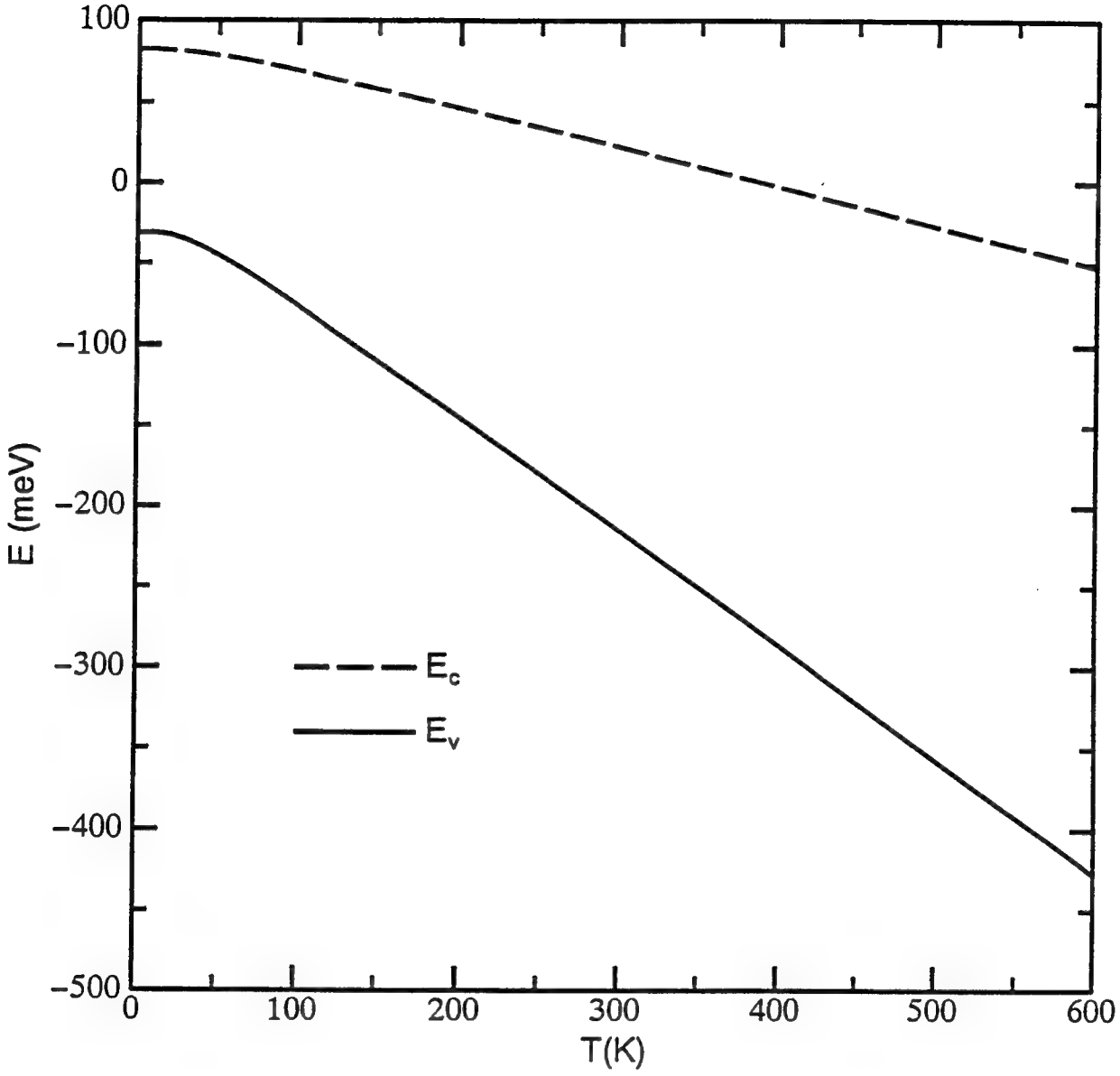
100
0
-100
-200
-300
-400
-500
E (meV)
0
100
200
300
400
500
600
T(K)
E_c
E_v

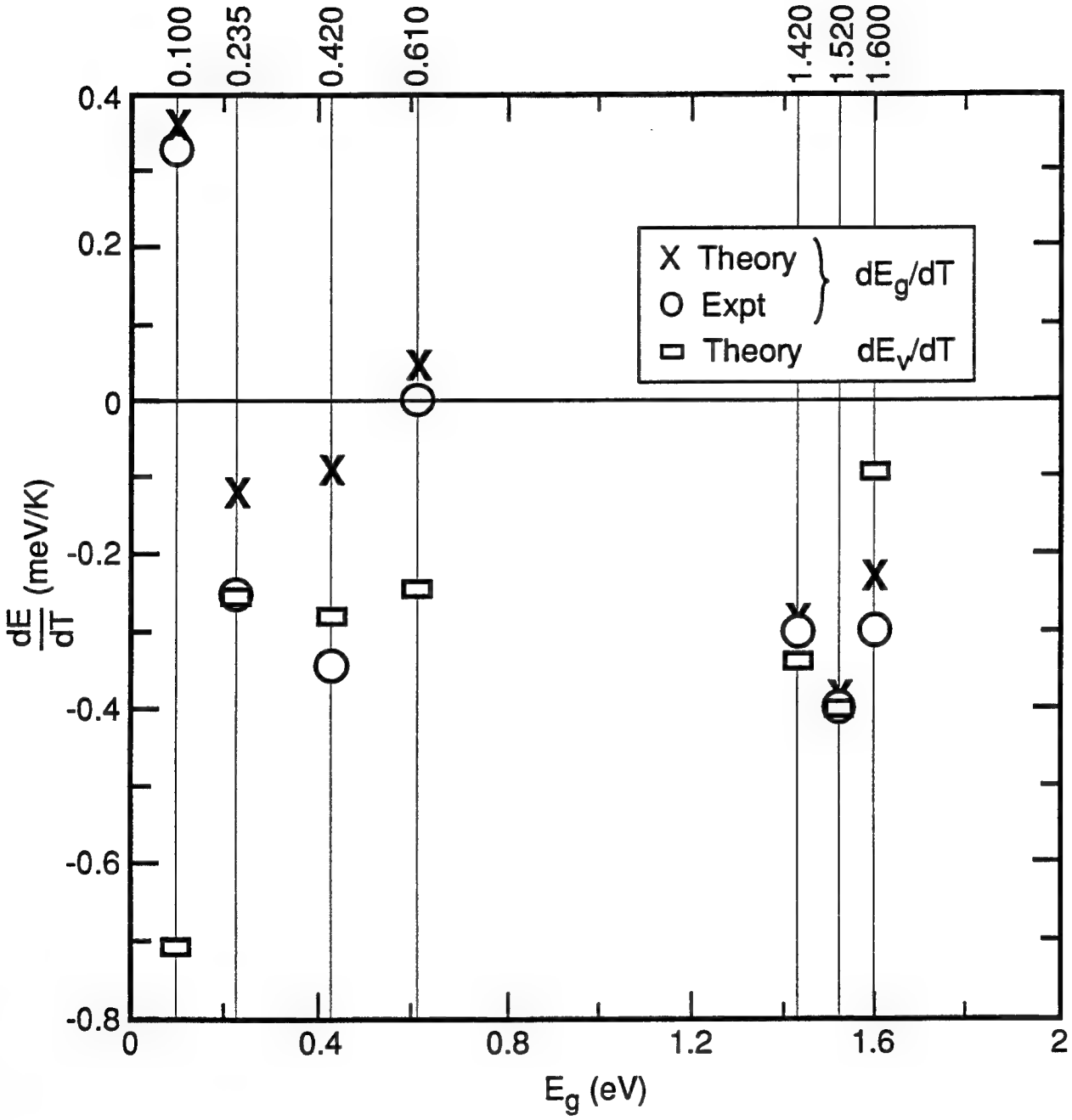
0.100
0.235
0.420
0.610
1.420
1.520
1.600
0.4
0.2
0
-0.2
-0.4
-0.6
-0.8
X Theory
O Expt
dEg/dT
Theory
dEv/dT
dE/dT (meV/K)
0
0.4
0.8
1.2
1.6
2
Eg (eV)

Appendix D

THEORETICAL EVALUATION OF InTlP, InTlAs, AND InTlSb AS LONG-WAVE INFRARED DETECTORS

THEORETICAL EVALUATION OF InTlP, InTlAs, AND InTlSb AS LONG-WAVE INFRARED DETECTORS

A. Sher, M. van Schilfgaarde, S. Krishnamurthy, and M.A. Berding
SRI International, Menlo Park, CA 94025
A.-B. Chen, Physics Department, Auburn University, AL 36849

ABSTRACT

We have evaluated three III-V semiconductor alloys—$In_{1-x}Tl_xP$ (ITP), $In_{1-x}Tl_xAs$ (ITA), and $In_{1-x}Tl_xSb$ (ITS)—as possible candidates for future long-wave infrared (LWIR) detector materials. The cohesive energies, elastic constants, band structures, electron mobilities, and phase diagrams are calculated and are compared to those of $Hg_{1-x}Cd_xTe$ (MCT) alloys. The band gaps of all three III-V alloys change from negative to positive values as the alloy composition x decreases from 1 to 0. The x values for the 0.1-eV gap are estimated to be 0.67, 0.15, and 0.08 respectively for ITP, ITA, and ITS. While both ITP and ITA form stable zincblende solid solutions for all alloy compositions, zincblende ITS is stable only for a range of x less than 0.15. The complication of the phase diagram in ITS is caused by the existence of a stable CsCl phase for pure TlSb. The alloy mixing enthalpies for ITP and ITA are comparable to those in MCT, and their phase diagrams should be qualitatively similar, characterized by simple lens-shape liquidus and solidus curves. Both ITP and ITA have considerably larger cohesive energies and elastic constants than those of MCT, indicating that they are structurally robust. At a 0.1-eV gap, the band structures near the gap and the electron mobilities in ITP, ITA, and ITS are also found to be comparable to those of MCT. Since the lattice constants of TlP and TlAs are less than 2% larger than the respective values in InP and InAs, the latter should provide natural substrates for the growth of active LWIR alloys, and offer a potential to integrate the detector array and read-out circuit.

We have proposed that the alloys $In_{1-x}Tl_xP$ and $In_{1-x}Tl_xAs$ have properties that distinguish them as outstanding candidates for IR electro-optic receiver and emitter devices.[1] This paper concentrates on the properties of $In_{1-x}Tl_xP$ in the long-wave infrared (LWIR) because it nearly lattice matches to InP substrates and, therefore, offers the prospect of integrated laser emitters, focal-plane-array (FPA) detectors, and read-out integrated circuits (ROIC) on the same chip. This capability could enable use of device architectures formerly deemed impractical because currently used LWIR materials are incapable of supporting them.

According to our first-principles theory, the following properties of TlP make it an attractive IR material candidate:

- It forms in the zincblende structure.
- Its lattice constant (5.96 Å) closely matches that of InP (5.83 Å) (so the pseudo-binary $In_{1-x}Tl_xP$ liquidus and solidus phase diagrams have simple lens shapes).
- Its cohesive energy per atom (2.56 eV/atom) is 58% greater than that of HgTe (1.62 eV/atom).
- It is a semimetal with a negative gap of -0.27 eV, about the same as that of HgTe (-0.3 eV).

The accompanying table presents the properties of the alloy with a 0.1-eV band gap that are related to LWIR-FPA performance and processing. The salient features are the following:

- The alloy concentration is x = 0.67, and the concentration variation of the gap |dEg/dx| is 1.42 eV, 16% smaller than that of $Hg_{0.78}Cd_{0.22}Te$ (1.69 eV).
- The elastic constants are ~33% larger than those of the LWIR HgCdTe alloy.
- The transverse optical phonon energy is 34.6 meV, 139% larger than that of HgCdTe (14.5), thereby limiting very-long-wave infrared (VLWIR) utility to $\lambda_c < 36$ μm (this is the only negative feature relative to HgCdTe).
- The temperature variation of the band gap[2] dE_g/dT near 77 K is small (~ -0.05 meV/K), about 1/7 as large as that of HgCdTe (0.36 meV/K) (dE_g/dT for $Hg_{1-x}Cd_xTe$ vanishes near x = 0.5, while that of $In_{1-x}Tl_xP$ vanishes close to x = 0.67, the LWIR concentration, greatly simplifying designs for variable temperature operation and eliminating spatial variation in pixel performance caused by temperature gradients over array areas).
- The electron effective mass is 0.008, almost identical to that of HgCdTe (~0.008).
- The hole effective mass is 0.37, 43% smaller than that of HgCdTe (0.65) (which implies higher hole mobilities and substantially longer electron Auger recombination lifetimes for InTlP).
- The electron mobility at 80 K ($6x10^4 cm^2/V\text{-}s$) is 44% smaller than that of HgCdTe, but it does not die off as rapidly as temperature increases; consequently, electron mobility at 200 K is $4.5x10^4 cm^2/V\text{-}s$, while the same for HgCdTe is $2.24x10^4 cm^2/V\text{-}s$, only half as large. (This means the high temperature responsivity should not degrade as rapidly in InTlP.)

---

[1] M. van Schilfgaarde, A.-B. Chen, S. Krishnamurthy, and A. Sher, *Appl. Phys. Lett.*, in press 1994.

[2] S. Krishnamurthy, A.-B. Chen, and A. Sher, submitted to *Appl. Phys. Lett.*, 1994.

ITA also has some virtues as an LWIR detector. While InAs is not as attractive a substrate as InP (bond energy per atom 3.10 eV) it is still better bound than CdTe (2.20 eV). The gap of TlAs is predicted to be -1.34 eV, so the LWIR concentration of $In_{1-x}Tl_xAs$ is x = 0.15. The predicted cohesive energy per atom of this alloy is 2.80 eV, far better than that of LWIR MCT (1.66 eV). Perhaps the most useful property of ITA is that its electron mobility falls very slowly as temperature increases, so at 200 °C LWIR ITA has $\mu_e = 0.5x10^4$ $cm^2/V\text{-}s$ compared to MCT with $\mu_e = 2.24x10^4$ $cm^2/V\text{-}s$. At still higher temperatures, the ratio of electron mobilities exceeds a factor of 10. Thus, minority carrier responsivities of p-type material may remain reasonably high at high temperature.

This collection of properties—plus the extra ease of processing, the lower defect densities expected as a consequence of the high cohesive energy, and the superior InP and InAs substrates (for InP there are 3-inch diameter wafers available with average dislocation densities of $\sim 10^4 cm^{-2}$)[3]—lends support to the contention that $In_{1-x}Tl_xP$ will prove to be a striking LWIR-FPA material, and there may be niches for $In_{1-x}Tl_xAs$.

ACKNOWLEDGMENTS

Partial support of this work from ONR Contracts N00014-88-C-0096 and N00014-89-K-0132 and from ARPA Contract MDA972-92-C-0053 is gratefully acknowledged.

[3]D.F. Bliss, R.M. Hilton, and J.A. Adamski, *Journal of Crystal Growth*, 128, 451, 1993.

LWIR MCT ITP AND ITA PROPERTIES COMPARISONS

Property		$Hg_{0.78}Cd_{0.22}Te$		$In_{0.33}Tl_{0.67}P$	$In_{0.85}Tl_{0.15}As$
		Theory	Experiment	Theory	Theory
1	$\overline{E}_g$ [eV]	0.1	0.1	0.1	0.1
2	$\overline{E}_b$ [eV/atom]	1.66	1.75	2.75	
3	$\overline{a}$ [Å]	6.45	6.46	5.92	6.08
4	$\hbar\omega_{To}$ [meV]	14.5	14.12	34.6	25.8
5	B[10^{12}erg/cm^3]	0.46	0.42	0.61	0.58
6a	dE_g/dx [eV] @ E_g (77 K) = 0.1 [eV]	1.71	1.69 @ 0 K	1.42	1.80
6b	dE_g/dT [meV/K]	0.36	0.3	~-0.05	—
7	m_e^* @ 0 K	0.008	~0.009	0.008	0.007
8	m_h^* @ 0 K	0.65	0.38-0.71	0.37	0.375
9	μ_e[cm^2/V-s]				
9a	@ 80 K	$1.07x10^5$	$0.986x10^5$	$6x10^4$	$1.16x10^5$
9b	@ 200 K	$2.24x10^4$	$2.0x10^4$	$4.5x10^4$	$6.72x10^4$
10	μ_h[cm^2/V-s]				
10a	@ 77 K	—	600-1400	—	—
10b	@ 200 K	—	300-600	—	
11a	τ_{eA}[ns] @ 10^{16} [cm^{-3}]	—	10	τ(MCT) < τ(ITP)	—
11b	τ_{hA}[ns]	—	40	—	—

Appendix E

LETTER TO PROFESSOR RAZEGHI

December 16, 1993

Professor M. Razeghi
Center for Quantum Devices
Department of Electrical Engineering
and Computer Sciences
Northwestern University
Evanston, ILL 60201

Dear Professor Razeghi,

Thank you for sending us a copy of Dr. Choi's thesis. I have read it with great interest. However, I am troubled by certain aspects of the experimental results and their interpretation. Let me begin by summarizing my interpretation of your group's results.

1. You have grown several epitaxial layers of InTlSb on InSb, and InSb buffered GaAs substrates. While you have not measured the Tl content of the layers, you observe an IR spectral absorption and photoconductive cut-off at 77°K for these layers that vary between that of pure InSb (5.5 μm) and 9.5 μm.

2. You find a linear relation between the average lattice constant of these layers determined by X-rays and the cut-off wave length (Figure 10). The maximum lattice constant percent difference with InSb is 1.4%.

3. From Figure 1, in Appendix E, the InTlSb layers have a smaller bond length than InSb.

4. The X-ray rocking curve width of the InTlSb layers tracks the apparent Tl content as judged by the lattice constant shift with InSb (Figure 11), and the widths are quite large indicating highly strained material.

There are other aspects to your data, but these four serve to illustrate my concerns.

If, for the moment, we assume you have grown homogenous layers of InTlSb, and as we have predicted, it only requires ~6% (possibly as much as 10%) Tl to narrow the gap to a 9.5 μm cut-off, then there is a serious problem. You measure a -1.4% lattice constant shift relative to InSb when $\lambda_c = 9.5$ μm. Therefore, this interpretation of your results requires that TlSb in the zincblende structure has a bond length that is -23% smaller than InSb (2.805 Å) or 2.16 Å. This bond length is smaller than that of Si (2.532 Å) and is quite unlikely. We predicted a 2% increase in the TlSb bond length relative to InSb. Thus, we would have to be in error by 25%. A table of our predictions compared to experiments for nearly all group IV, III-V compounds, and II-VI compounds is enclosed. Please note that the predicted bond lengths all fall within 1% of experiment. It is hard to fathom why the only semiconductor compound we get wrong by 25% is TlSb.

Your results may be at least partly explained if we assume your growth at 450° C was done above the eutectic temperature. Then the layers would be inhomogenous, their bulk being zincblende $In_{1-x}Tl_xSb$ with $x \cong 0.01$ and there would TlSb inclusions of material in the CsCl (or possibly NaCl) structure. These inclusions would have short bond lengths and, of course, higher coordination numbers (CsCl is 8 and NaCl is 6). Thus, they would stress or even disorder in the surrounding material which may account for the bandgap reduction. We have seen from electronic structure calculations that the local gap is very sensitive to lattice distortions.

Can your X-ray data be interpreted as InSb plus smaller lattice constant TlSb inclusions? Can the large X-ray rocking curve width variations be due to increasing inclusion content as the Tl content is increased? Have you looked for inclusions with TEM or even an EBIC attachment to an SEM? If you find inclusions, then the obvious corrective action is to lower your growth temperature below the eutectic temperature, thereby growing homogenous layers.

Obviously something is wrong here. The observed bond length variations are highly improbable for a homogenous zincblende material. Quite aside from our theoretical predictions, it is unlikely that the TlSb bond length is smaller than that of Si. If you are actually growing two phase inhomogenous material, and the cut-off wave length shift is caused by strain, then at least some aspects of the results would be explained and it is easy to see how to correct the situation. That contention is, however, quite speculative and needs to be tested. If your material proves to be homogenous, then we are for now at a loss to understand your experimental results.

Sincerely yours,

Arden

Arden Sher
Associate Director
Physical Electronics Laboratory

Enclosure

cc: R. Balcerak
S.Y. Park
G. Wright